Clays and Clay Minerals, Vol. 57, No. 5, 649–671, 2009.

THE CHARGE OF COMPONENT LAYERS OF ILLITE-SMECTITE IN BENTONITES AND THE NATURE OF END-MEMBER ILLITE

JAN ŚRODOŃ[1,*], EDWIN ZEELMAEKERS[2,†], AND ARKADIUSZ DERKOWSKI[1,†]

[1] Institute of Geological Sciences PAN, Senacka 1, 31002 Krakow, Poland
[2] Laboratory for Applied Geology and Mineralogy, University of Leuven, Celestijnenlaan 200E, 3001 Heverlee, Belgium

Abstract—The nature of component layers of mixed-layer illite-smectite and their possible evolution in the course of illitization have been debated since the 1960s. The present study is a new attempt to solve these problems, using samples collected from diverse geological formations around the world. Twenty three purified illite-smectites from bentonites and hydrothermal rocks, covering the complete range of expandability, were analyzed chemically, including NH_4^+ determination, and their structural formulae were calculated. The exchangeable cations (EXCH) were plotted *vs.* the fixed cations (FIX) yielding the following experimental regression:

$$EXCH = -0.43 \times FIX + 0.41 \quad (R^2 = 0.98)$$

FIX and EXCH depend on the charge of the illite (Q_i) and smectite (Q_s) interlayers, and the fractions of these interlayers in the bulk clay leading to:

$$EXCH = -Q_s/Q_i \times FIX + Q_s$$

Analysis of these relations and independent measurements of the total specific surface area (TSSA) indicate that the layer charges of both types do not change in the course of illitization. The smectite layer charge is equal to 0.41 and the illite layer charge is equal to 0.95 per $O_{10}(OH)_2$. End-member illite has a well defined composition that is close to intermediate between muscovite and phengite, with fixed cations content greater than that specified in the AIPEA classification of layer silicates:

$$FIX_{0.95}(Si_{3.25}Al_{0.75})(Al_{1.81}Fe_{0.01}Mg_{0.19})O_{10}(OH)_2$$

The established relationship allows the calculation of the mean number (N) of 2:1 layers in all fundamental particles and also the fraction of smectitic layers (f_s) from FIX:

$$N = Q_i/(Q_i - FIX) \quad f_s = (Q_i - FIX)/Q_i$$

N and f_s can be used to calculate TSSA, and all three parameters can also be calculated from cation exchange capacity and from X-ray diffraction peak positions, utilizing the regressions established here.

Key Words—CEC, Charge Density, EGME, Illite, Illite-smectite, Layer Charge, NEWMOD, Smectite, Specific Surface Area, Surface Area, Water Sorption, XRD.

INTRODUCTION

Attempts to characterize the chemistry of the component layers of illite-smectite (I-S) began with that by Mehra and Jackson (1959), who concluded from K_2O and surface-area measurements of illites that all K_2O comes from the non-expandable (illitic) layers and all samples with <10 wt.% K_2O contain some expandable layers. Weaver (1965) made the first attempt to calculate the smectitic and illitic components from the overall structural formula of illite-smectite and the layer ratio evaluated by XRD. A smectitic layer charge (Q_s) of $0.46/O_{10}(OH)_2$ and an illitic layer charge (Q_i) of 0.84 were established, similar to the $Q_s = 0.36$ and $Q_i = 0.88$ established by Brown and Weir (1963) for rectorite.

The first systematic chemical study of a series of illite-smectites was published by Hower and Mowatt (1966), who plotted fixed cations (FIX = K+Na) *vs.* percent of smectite layers evaluated by XRD ($\%S_{XRD}$) and obtained by linear extrapolation $Q_i = 0.75$. Those authors concluded that the illite end-member of the mixed-layer series was a mineral species distinct from true mica, and observed that cation exchange capacity (CEC) correlates well with $\%S_{XRD}$. Środoń *et al.* (1986) using a similar approach on a broader set of samples, covering the entire range of $\%S_{XRD}$, found that the FIX *vs.* $\%S_{XRD}$ relationship is not linear but concave, and suggested that it was due to the presence of two types of illite layers with $Q_i = 0.55$ in random (R0) I-S and $Q_i = 1.00$ in ordered (R >0) I-S.

Velde and Brusewitz (1986) concluded from chemical and XRD data that $Q_i = 0.7$ and that Q_s is stable during illitization, but varies from 0.3 to 0.7 between different sample sets. Meunier and Velde (1989) arrived at similar conclusions by chemiographic analysis: $Q_s = 0.33-0.66$ and $Q_i = 0.87$. Different relationships were found for soil-derived I-S, using a non-linear optimization of chemical data (Laird *et al.*, 1991): $Q_s = 0.48$ and $Q_i = 0.47$.

Nadeau and Bain (1986) were the first to measure ammonium as a minor fixed cation in I-S and the first to observe that XRD appears to overestimate the proportion of illite layers, compared to direct TEM measurements of

* E-mail address of corresponding author:
ndsrodon@cyf-kr.edu.pl
† Present address: Chevron ETC, 3901 Briarpark, Houston, TX, USA
DOI: 10.1346/CCMN.2009.0570511

the thickness of fundamental particles. Their results suggested that Q_i and Q_s are similar and that they increase in the course of illitization from ~0.5 to ~0.9. Środoń *et al.* (1992) also used transmission electron microscopy to calculate %*S*, but found that Q_i and Q_s are stable at 0.89 and 0.4, respectively. Identical values were obtained by Ylagan *et al.* (2000), who applied the same technique to a set of I-S samples from a hydrothermal alteration zone. Loucks (1991) suggested that the vacant illite interlayer sites (Q_i <1.00) were occupied by hydronium and molecular water, or by molecular water only (Slonimskaya *et al.*, 1978; Drits and McCarty, 2007). The most recent report of the AIPEA Nomenclature Committee dealing with clay nomenclature (Guggenheim *et al.*, 2006) defined illite as 'interlayer-deficient mica' with a layer charge of 0.6–0.85.

Cetin and Huff (1995) used the alkylammonium technique to investigate the expandable layer charge during diagenesis and concluded that at ~10%S_{XRD} it changes from smectitic to vermiculitic. Sato *et al.* (1996) carried out a similar study using several tests (K-saturation, Greene-Kelly test, alkylammonium) and concluded that smectite becomes more beidellitic before the onset of illitization; its layer charge increases from 0.28 to 0.37, and this process continues during illitization. Meunier *et al.* (2000), analyzing a broad range of published data, came to the conclusion that in the course of diagenesis smectite layers first evolve into vermiculite layers and then undergo illitization.

Review of the literature suggests that the nature of the component layers of I-S is still ambiguous, along with their evolution during illitization. The results of another attempt to solve this puzzle are presented below, and built on the results of Środoń and McCarty (2008), who demonstrated how to use CEC and H_2O and EGME sorption for an accurate measurement of the layer charge and the total specific surface area (TSSA) of pure smectites. Combining this approach with a careful chemical analysis of a broad set of pure samples offers a new insight into the crystal chemistry and evolution of I-S. Most of the symbols used in this paper were defined in the appendix of the paper by Środoń and McCarty (2008).

MATERIALS AND METHODS

Twenty three samples or rocks containing I-S of different layer ratios, and possibly free of other mineral admixtures, were selected for this study. Most are bentonites of various ages and a few come from a hydrothermal clay deposit in Hungary. Two reference smectites (Wyoming and Cheto) were also studied. Table 1 lists the details and gives relevant references.

The rocks were crushed in a hand mortar and treated chemically to remove carbonates, organic matter, and Fe oxides (Jackson, 1975). After initial removal of the excess electrolyte by centrifugation, the <0.2 μm fractions were separated. A small portion was then coagulated with NaCl, while most of the clay suspension was converted into Ca form by four exchanges with 1 N $CaCl_2$. Both Na and Ca clays were purified by centrifugation followed by dialysis, monitored by a conductometer, and finally freeze dried. The purity of the clay fractions was checked by X-ray diffraction (XRD), using side-loaded, random preparations. The XRD identification of illite-smectite was performed using 4.5 cm long sedimented preparations (10 mg clay/cm^2), under conditions of ethylene-glycol saturation and after dehydration by heating. The XRD patterns of the oriented Ca-saturated preparations were registered over a 2–50º2θ CuKα range for 3 s/0.02º2θ step on a Thermo X'tra diffractometer equipped with two Soller 1.3º slits, 0.9 mm divergent slit, 0.3 mm receiving slit, 1.05 mm divergent scatter slit, and 1 mm receiving scatter slit. The peak positions were found to be accurate within ±0.02º2θ, based on quartz impurities present in a few samples. The oriented slides of K-saturated samples spiked with silicon powder (NIST standard SRM 640c) were heated at 150ºC and 250ºC and immediately registered under N_2 atmosphere over a 2–52º2θ CuKα) range using 5 s/0.01º2θ steps on a Thermo X'tra diffractometer equipped with two Soller 2º slits, 0.8 mm divergent slit, 0.2 mm receiving slit, 4 mm divergent scatter slit, and 0.5 mm receiving scatter slit.

The loss on ignition of Na and Ca samples (from the air-dry state to 1 h at 1100ºC) and the %K_2O of the ignited Ca samples (Sherwood Model 420 flame photometer) were measured. The total specific surface area (TSSA) was measured by a technique combining the approach used by Tiller and Smith (1990, free surface EGME sorption) and Newman (1983, water sorption). Clay samples in Ca form were first equilibrated at 47% RH over a saturated solution of lithium nitrate. After overnight equilibration, all samples were weighed and placed in the desiccator again. Next, the weight of H_2O released during heating to 200ºC followed by isothermal heating at 200ºC for 0.5 h was established using a programmable thermobalance, and the hot sample was placed in the desiccator used for the EGME determination. After equilibrating all samples with EGME, the sample weights were measured again. Using this approach, sorption of both H_2O and EGME can be referred to the same weight of clay, obtained at 200ºC, which is close to the absolutely dry weight, thus independent of changes in relative humidity (Środoń and McCarty, 2008). Finally, the CEC was measured by the Co-hexamine technique of Orsini and Remy (1976) and Bardon *et al.* (1983) on the same sample split, and referred to the same weight at 200ºC. The optimum Co-hexamine solution concentration was estimated from the sorption data. Testing performed on separate sample splits proved that CEC measured on EGME samples is essentially the same as measured on the H_2O samples ($CEC_{EGME} = 0.998 \times CEC_{H_2O} + 2.15$, $R^2 = 0.998$).

https://doi.org/10.1346/CCMN.2009.0570511 Published online by Cambridge University Press

Major element analysis was performed by inductively coupled plasma mass spectrometry (ICP-MS) on ignited Ca samples fused with a Li metaborate-tetraborate flux at Activation Laboratories, Canada. NIST 70a (K feldspar) and 76a (burnt refractory) standards were used to check the accuracy of these analyses.

The same laboratory measured the C, N, and S contents by LECO CNS-2000 from air-dry Na samples and the major element contents, including Co, by the Li metaborate-tetraborate fusion XRF technique on the samples after the Co-hexamine exchange and purification by dialysis.

Fourier-transform infrared (FTIR) spectroscopy of selected samples was conducted using the KBr pellet technique. The pellets (0.8 mg sample/300 mg potassium bromide) were prepared by dehydration of the clays (by heating for 24 h at 110ºC) and of the KBr powder (by heating for 24 h at 550ºC). The pellets were further dehydrated by storing at 195ºC overnight. The spectra were recorded in a dry N_2 atmosphere using a Fourier Transform Infrared Spectrometer Bio Rad FTS 135. For each sample 32 scans were collected in the range 400−4000 cm^{-1} at a resolution of 2 cm^{-1}.

RESULTS

Chemical analyses, independent checks for the presence of NH_4^+, and structural formulae

All of the original chemical analyses and the mineral impurities detected by XRD are listed in Table 1. The accuracy and precision of the ICP data were checked by triple analyses of two NIST standards. The analyses were found to be within 5 relative % of the certified values for all components >1%, except for K_2O, for which the error reached 9 relative %. Most errors were random; only Al_2O_3 and K_2O contents were found to be systematically underestimated. Al_2O_3 data were then increased by 3 relative %, which is a correction factor based on the certified and the measured values for the two NIST standards. The K_2O data obtained by flame photometry were used, which for the two NIST standards fall within the certified values. The following correlation between the two K_2O data sets was established (both obtained for ignited samples):

$$\%K_2O\ (FP) = 1.036 \times \%K_2O\ (ICP) + 0.0893 \qquad R^2 = 0.996$$

The precision of the C, N, and S measurements was checked by double analyses of six samples and found to be within 0.03% absolute for C and 0.01% for N and S.

The C contents of all samples were found to be <0.2%. The N content of bituminous coals, which corresponds to the range of diagenesis studied, does not exceed 2% (Burchill and Welch, 1989). N can, therefore, be considered as representing inorganic ammonium fixed in illite and the %N in air-dry Na-samples can be recalculated to $\%(NH_4)_2O$ in the ignited sample and added to the silicate major elements.

To validate these assumptions, two independent methods (FTIR and XRD) were used to check for the presence of NH_4^+ in the illite interlayer space. Six samples (with large and small N contents) were analyzed by FTIR and the spectra were consistent with the chemical data: the intensities of NH_4^+ bands at 1430, 3048, and 3307 cm^{-1} are proportional to the $\%(NH_4)_2O$ established from chemical analysis (Figure 1).

For five heated, K-saturated samples (four NH_4^+ -rich and one NH_4^+ -poor), *d* spacing and peak-profile analyses were carried out on oriented XRD patterns, following the method proposed by Drits *et al.* (1997a, 2005). This method requires the slides to be heated at 150ºC and warns against the use of temperatures which are too high (300ºC). Because one sample (Małe Ciche) clearly did

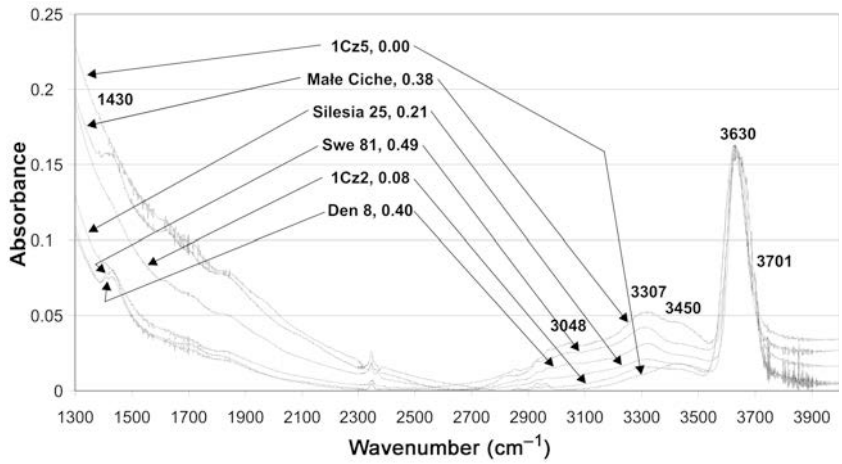

Figure 1. FTIR spectra of dehydrated KBr discs of <0.2 μm fractions, illustrating the complete range of detected substitution of NH_4^+ (the bands at 1430, 3048, and 3307 cm^{-1}) for K^+. The spectra are normalized to the OH-stretching band at 3630 cm^{-1} after removing a flat background. The percentage of $(NH_4)_2O$ from Table 1 is reported next to the sample names. A residual water band can be observed at 3450 cm^{-1} and a kaolinite band (Silesia 25) at 3701 cm^{-1}.

https://doi.org/10.1346/CCMN.2009.0570511 Published online by Cambridge University Press

Table 1. Chemical and XRD data for illite-smectite samples, two reference smectites and two NIST standards.

Sample	SiO_2 (%)	Al_2O_3 (%)	CaO (%)	MgO (%)	Na_2O (%)	K_2O (%)	$(NH_4)_2O$ (%)	Fe_2O_3 (%)	MnO (%)	TiO_2 (%)	P_2O_5 (%)	Total (%)	LOI (Ca) (%)	C (%)	N (%)	S (%)	H_2O (mg/g)	EGME (mg/g)	CEC (meq/100 g)	f_{CaO}	Impurities	d_{06} (Å)
Nor 27[1]	54.49	28.49	0.78	2.93	0.27	8.54	0.14	2.56	0.010	0.630	0.13	99.11	8.38	0.04	0.07	<0.01	47.3	82.3	16.75	0.02	Ch, Ab, A, Q	1.501
Fuzz 6[2]	55.23	31.12	0.82	2.51	0.03	8.82	0.06	0.36	0.005	0.027	0.03	99.07	10.62	0.06	0.03	<0.01	68.1	115.6	26.62	0.05	–	1.499
Swe 151[1]	56.88	29.41	0.98	3.12	0.06	7.44	0.43	1.10	0.007	0.085	0.04	99.98	11.66	0.05	0.21	<0.01	76.3	145.0	27.69	0.26	–	1.501
Swe 162[1]	56.68	29.96	0.98	2.64	0.06	7.28	0.45	1.35	0.005	0.131	0.05	100.03	10.69	0.08	0.22	0.01	73.8	125.4	28.59	0.02	–	1.500
Fuzz 5[2]	54.68	32.68	0.97	1.52	0.02	8.65	0.06	0.26	0.015	0.062	0.03	99.01	11.42	0.11	0.03	<0.01	71.6	119.5	28.56	0.00	–	1.497
Swe 81[1]	56.13	29.92	0.96	2.26	0.09	6.97	0.49	1.50	0.004	0.672	0.05	99.54	11.54	0.08	0.24	0.02	70.7	143.9	29.98	0.05	A, Q	1.500
Fuzz 9[2]	55.10	31.78	0.88	2.30	0.04	8.61	0.04	0.24	0.007	0.050	0.04	99.13	10.20	0.04	0.02	<0.01	56.6	121.0	25.68	0.03	–	1.497
Fuzz 3[2]	56.08	30.33	0.93	2.86	0.04	8.28	0.08	0.34	0.010	0.063	0.05	99.15	11.13	0.19	0.04	<0.01	67.7	119.0	29.40	0.03	–	1.498
Den 8[1]	54.93	30.90	1.10	1.59	0.11	6.93	0.40	1.46	0.011	0.601	0.08	98.51	11.54	0.18	0.19	0.74	70.2	134.8	30.51	0.01	Py, A, Q	1.498
Zukowice 2[3]	59.24	26.20	1.40	3.60	0.04	6.62	0.13	1.47	0.006	0.177	0.05	99.05	14.68	0.11	0.06	0.05	100.0	168.4	39.70	0.06	Q, Ch	1.500
Est 62[1]	60.91	22.71	1.34	4.47	0.05	6.26	0.02	2.60	0.002	0.100	0.02	98.50	14.37	0.08	0.01	0.01	104.7	195.2	46.03	0.01	–	1.500
Swe 84[1]	61.15	23.05	1.40	3.56	0.13	5.74	0.13	2.49	0.006	0.233	0.02	98.03	15.07	0.05	0.06	<0.01	114.4	201.1	44.47	0.04	–	1.501
Małe Ciche 5[4]	55.55	32.06	1.90	1.58	0.45	4.34	0.38	1.41	0.006	0.616	0.05	98.72	14.56	0.11	0.18	0.01	110.6	188.7	55.64	0.05	A, Ch	1.497
Silesia 25[5]	58.98	28.58	1.68	2.50	0.10	4.83	0.21	0.93	0.004	0.105	0.03	98.16	14.78	0.10	0.10	0.02	117.5	182.3	53.65	0.04	K, Q	1.499
Ch3[5]	60.94	25.55	1.65	3.49	0.11	5.13	0.17	2.61	0.006	0.057	0.03	99.91	14.75	0.11	0.08	<0.01	107.1	196.1	50.39	0.03	–	1.500
Ch4[5]	60.11	26.23	1.77	3.05	0.11	4.93	0.12	2.52	0.019	0.043	0.04	99.07	14.69	0.05	0.06	<0.01	115.4	189.5	54.02	0.05	Q	1.500
1M4[5]	61.69	25.01	1.99	3.08	0.09	4.28	0.06	2.85	0.004	0.051	0.03	99.20	14.47	0.07	0.03	<0.01	125.9	204.1	65.97	0.05	–	1.498
CIC 1/20[6]	60.07	27.65	2.41	2.42	0.16	3.13	0.11	3.21	0.015	0.192	0.06	99.53	15.12	0.04	0.05	<0.01	142.7	224.3	77.78	0.05	Ch, Q	1.499
Mikołów 27[5]	61.84	24.84	2.36	3.16	0.12	3.13	0.06	3.12	0.004	0.134	0.04	98.88	18.19	0.06	0.03	<0.01	147.4	235.0	75.62	0.03	K	1.499
1Cz2[5]	63.80	24.26	2.40	3.45	0.11	2.78	0.08	3.11	0.004	0.058	0.03	100.17	14.98	0.03	0.04	<0.01	137.3	228.2	78.80	0.03	K	1.498
2M2[5]	63.37	23.74	2.39	3.33	0.12	2.67	0.06	3.01	0.004	0.064	0.03	98.85	13.59	0.05	0.03	<0.01	150.5	228.0	82.01	0.01	–	1.497
2M3[5]	65.00	23.09	2.92	3.58	0.11	1.66	0.04	3.21	0.009	0.056	0.04	99.76	16.45	0.07	0.02	<0.01	168.9	256.8	92.78	0.01	–	1.498
1Cz3[5]	65.28	22.74	2.85	3.57	0.12	1.28	0.02	3.65	0.004	0.057	0.01	99.60	14.06	0.03	0.01	<0.01	167.4	261.9	93.02	0.03	–	1.497
2M6[5]	66.12	22.61	2.95	3.74	0.14	0.82	0.04	3.32	0.006	0.085	0.02	99.90	14.33	0.07	0.02	<0.01	175.9	276.7	97.15	0.01	–	1.498
1Cz5[5]	66.20	22.83	3.12	3.68	0.11	0.43	0.00	3.08	0.009	0.063	0.02	99.54	15.98	0.04	<0.01	<0.01	171.6	278.7	101.07	0.01	–	1.496
1Cz4[5]	66.03	21.97	3.06	3.73	0.13	0.31	0.00	3.42	0.007	0.054	0.02	98.73	15.54	0.06	<0.01	<0.01	178.6	292.7	99.73	0.01	–	1.496
Wyoming[7]	66.30	22.74	2.97	2.73	0.06	0.20	0.00	4.66	0.003	0.094	0.02	99.78	18.09	0.21	<0.01	<0.01	161.4	300.4	84.97	0.00	–	1.497
Cheto[7]	67.93	20.07	3.79	5.98	0.13	0.17	0.05	1.78	0.007	0.242	0.03	100.22	23.45	0.08	0.02	<0.01	211.4	334.4	123.12	0.02	–	1.498
NIST 70a	67.28	16.86	0.13	0.04	2.53	11.90	0.00	0.08	0.002	0.005	<0.01	98.83	0.78	<0.01	<0.01	<0.01						
NIST 76a	54.67	37.92	0.21	0.49	0.05	1.34	0.00	1.58	0.002	2.008	0.13	98.40	1.04	<0.01	<0.01	<0.01						

LOI – loss on ignition for Ca-exchanged samples, H_2O – water retention at 47% RH, EGME – EGME retention, f_{CaO} – fraction of CaO left in clay after Co-hexamine exchange, Ch – chlorite, Ab – albite, A – anatase, Q – quartz, K – kaolinite, Py – pyrite.

[1] Ordovician bentonites from the Baltic Basin (Bergström *et al.*, 1995), [2] Miocene hydrothermal clays from Fuzzeradvany, Hungary (Viczián, 1997), [3] Silurian bentonite from SE Poland, [4] Miocene bentonite from Podhale Basin, Poland (Środoń *et al.*, 2006a), [5] Carboniferous bentonites from the Upper Silesia Coal Basin, Poland (Środoń *et al.*, 2006b), [6] Miocene bentonite from the East Slovak Basin (Clauer *et al.*, 1997), [7] CMS standards.

not collapse entirely at 150ºC, all samples were reheated at 250ºC and recorded again. At this temperature, the Małe Ciche sample collapsed but did not change the peak positions and shapes of the other samples. The latter set of data was used in the calculations.

The angle-corrected peak breadth (full width at half maximum – FWHM, multiplied by the cosine of the Bragg angle in ºθ of that particular peak) increased with increasing *l* (Table 2). Drits *et al.* (2005) demonstrated that this is indicative of the interstratification of 9.98 Å K layers (illite layers) and separate 10.33 Å NH_4^+-layers (tobellite layers), as opposed to the situation where K^+ and NH_4^+ are distributed within the interlayers. This means that the NH_4^+-bearing I-S should, in fact, be considered as three-component illite-tobellite-smectite.

Using equation 2 from Drits *et al.* (2005), the fractions of NH_4^+ interlayers were calculated from the *d* spacings of the 005 reflections. The results confirm the presence of fixed NH_4^+ for four NH_4^+-rich samples, and for three of these agree well with the evaluation based on chemistry and modeled expandabilities (Table 2). The sensitivity of this technique was insufficient to detect the small amount of fixed NH_4^+ in sample Nor 27.

The S content from chemical analysis was used to calculate pyrite content and subsequent wt.% Fe_2O_3, which was subtracted from the chemical analysis. These corrections were <0.1% except for sample Den 8, which contained 1.05% pyrite, clearly detectable by XRD (Figure 2). The TiO_2 content is quite scattered (Table 1) and was assigned to anatase, consistent with the XRD data (Table 1, Figure 2). The very stable P content (Table 1) was assumed to be from apatite and the analyses were corrected for %CaO corresponding to a typical sedimentary apatite composition ($0.55CaO/0.40P_2O_5$).

Four I-S samples contained measurable admixtures of other minerals. Based on the relative intensities of relevant XRD reflections, the composition of sample Nor 27 was corrected for 1% of Fe-Mg chlorite and 1% of quartz; Silesia 25 for 2% of kaolinite and 1% of quartz; Małe Ciche for 1% of chlorite; and CIC 1/20 for 1.5% of Fe-Mg chlorite and 1% of quartz. The chlorite corrections resulted in removal of traces of Mg originally assigned to I-S interlayer cations. Per analogy, 0.5 and 0.3% of Fe-Mg chlorite were removed from the chemical compositions of samples Swe 151 and Fuzz 3, respectively, which also contained traces of interlayer Mg. An *Excel*™ spreadsheet was built, which allowed manipulation of chemical data for all samples simultaneously, and the resulting structural formulae were plotted. The relations of fixed cations per $O_{10}(OH)_2$ ($FIX = K^+ + Na^+ + NH_4^+$) and exchangeable cations ($EXCH = 2*Ca^{2+}$), critical for this work (Figure 3), were used as a test. Such an assumption about FIX and EXCH, following Środoń and McCarty (2008), is considered a good approximation, since the samples studied were saturated carefully with Ca^{2+} cations. All the corrections introduced changed the experimental regression only at the third decimal place and improved the R^2 of the regression only at the second decimal place. Introducing 25% Fe^{2+} also had a negligible effect. The trends reported below, which are based on the calculated structural formulae, are therefore, very reliable.

The calculated I-S formulae (Table 3) all have sums of octahedral cations between 1.98 and 2.00, except sample Swe 84 (1.96). After the chlorite corrections, no

Table 2. Peak positions (º2θ), *d* spacings, peak width at half maximum (FWHM) of K-saturated and heated (250ºC) samples, and fixed NH_4^+ as percentages of all interlayers calculated from d_{005} using equation 2 from Drits *et al.* (2005), and calculated from NH_4^+ as a percentage of FIX (Table 3) and %S (high-angle fitting – haf) from Table 5.

	Reflection	º2θ	*d* (Å)	FWHM (º2θ)	Cos(ºθ) × FWHM	%NH_4^+ (XRD)	%NH_4^+ (chem)
Swe 81	002	17.68	5.0163	0.70	0.69		
	003	26.77	3.3301	0.78	0.76		
	005	45.33	2.0005	0.99	0.91	8	9
Swe 162	002	17.69	5.0135	0.58	0.57		
	003	26.77	3.3301	0.70	0.68		
	005	45.34	2.0001	0.90	0.83	7	8
Swe 151	002	17.71	5.0079	0.64	0.63		
	003	26.80	3.3264	0.73	0.71		
	005	45.38	1.9984	0.94	0.87	5	8
Den 8	002	17.64	5.0276	0.71	0.70		
	003	26.71	3.3374	0.78	0.76		
	005	45.24	2.0043	1.00	0.92	13	7
Nor 27	002	17.79	4.9856	0.58	0.57		
	003	26.86	3.3191	0.61	0.59		
	005	45.49	1.9939	0.73	0.67	0	3

https://doi.org/10.1346/CCMN.2009.0570511 Published online by Cambridge University Press

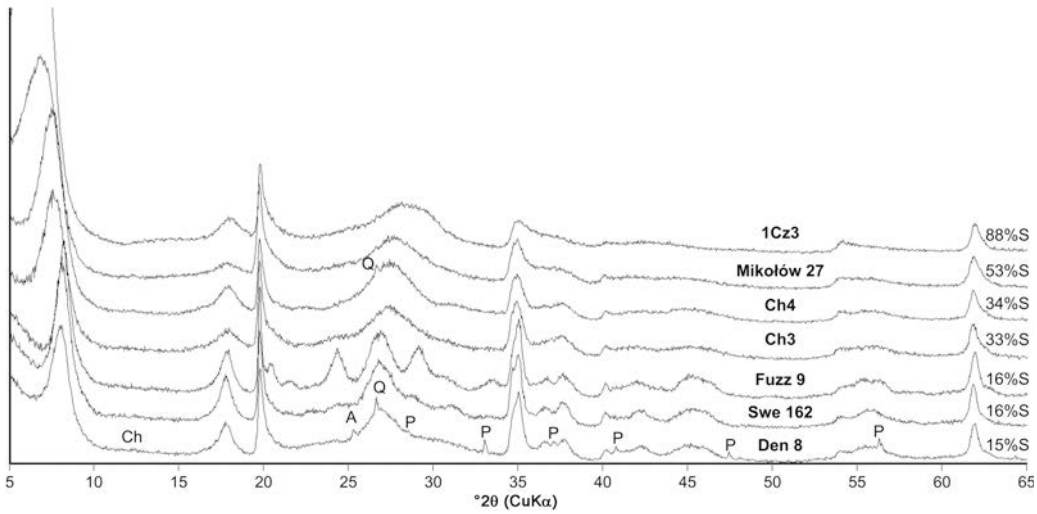

Figure 2. XRD patterns of side-loaded, random preparations of <0.2 μm fractions illustrating the evolution of tridimensional organization of illite-smectites with decreasing percentage of smectite layers ($\%S_{XRD}$), and the level of contamination by other minerals: Ch – chlorite, A – anatase, Q – quartz, P – pyrite.

Mg was found in excess of the dioctahedral occupancy, except for the reference Cheto montmorillonite sample. Compositional trends in the course of illitization were traced by plotting different components *vs.* FIX (Figure 3). Scattered linear positive trends were observed for Al^{VI} and NH_4^+ and negative trends for Fe

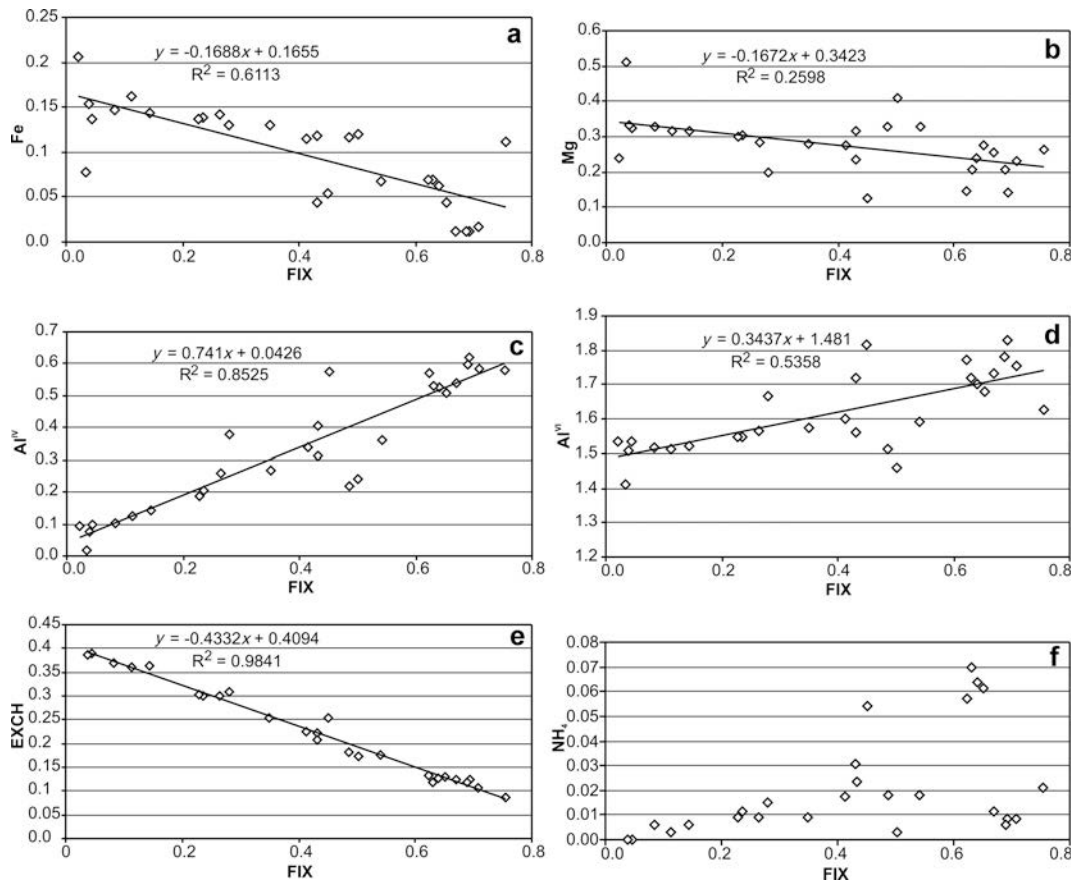

Figure 3. Chemical evolution during illitization: plots of different components of structural formulae of I-S *vs.* fixed cations (FIX). Data from Table 3.

https://doi.org/10.1346/CCMN.2009.0570511 Published online by Cambridge University Press

Table 3. Structural formulae, total specific surface area (TSSA) and fraction of smectitic layers (f_s) calculated from H_2O and EGME sorption. %diff is the percent difference from $TSSA_{Nr}$ value in Table 4. The f_s >1 for Cheto indicate that the coverages selected for the I-S series are too small in the case of this high-charge smectite.

Sample name	Tetrahedral		Octahedral				Interlayer														
	Si	Al^{IV}	Al^{VI}	Fe^{3+}	Mg	Sum VI	Ca	Na	K	Mg	NH_4	Q	EXCH	FIX	NH_4 as % of FIX	TSSA (H_2O) (m^2/g)	%diff from $TSSA_{Nr}$ (%)	$f_S(H_2O)$	TSSA (EGME) (m^2/g)	%diff from $TSSA_{Nr}$ (%)	f_S (EGME)
Nor 27	3.42	0.58	1.63	0.11	0.26	2.00	0.04	0.03	0.70	0.00	0.02	0.84	0.09	0.75	3	189	25	0.25	200	33	0.26
Fuzz 6	3.42	0.58	1.75	0.02	0.23	2.00	0.05	0.00	0.70	0.00	0.01	0.81	0.11	0.71	1	272	45	0.36	281	50	0.37
Swe 151	3.49	0.51	1.68	0.04	0.27	2.00	0.06	0.01	0.58	0.00	0.06	0.78	0.13	0.65	9	305	30	0.40	353	51	0.46
Swe 162	3.47	0.53	1.70	0.06	0.24	2.00	0.06	0.01	0.57	0.00	0.06	0.77	0.13	0.64	10	295	21	0.39	305	25	0.40
Fuzz 5	3.38	0.62	1.83	0.01	0.14	1.98	0.06	0.00	0.68	0.00	0.01	0.82	0.12	0.69	1	286	43	0.37	291	46	0.38
Swe 81	3.47	0.53	1.72	0.07	0.21	2.00	0.06	0.01	0.55	0.00	0.07	0.75	0.12	0.63	11	283	12	0.37	350	39	0.46
Fuzz 9	3.40	0.60	1.78	0.01	0.21	2.00	0.05	0.00	0.68	0.00	0.01	0.81	0.12	0.69	1	226	11	0.30	294	45	0.38
Fuzz 3	3.46	0.54	1.73	0.01	0.25	2.00	0.06	0.00	0.65	0.00	0.01	0.79	0.12	0.67	2	271	24	0.35	290	32	0.38
Den 8	3.43	0.57	1.77	0.07	0.15	1.99	0.07	0.01	0.55	0.00	0.06	0.75	0.13	0.62	9	281	9	0.37	328	27	0.43
Zukowice 2	3.64	0.36	1.59	0.07	0.33	1.99	0.09	0.00	0.52	0.00	0.02	0.72	0.18	0.54	3	400	24	0.52	410	27	0.54
Est 62	3.76	0.24	1.46	0.12	0.41	1.99	0.09	0.01	0.49	0.00	0.00	0.68	0.17	0.50	1	419	18	0.55	475	34	0.62
Swe 84	3.78	0.22	1.51	0.12	0.33	1.96	0.09	0.02	0.45	0.00	0.02	0.67	0.18	0.49	4	458	24	0.60	489	33	0.64
Małe Ciche 5	3.42	0.58	1.82	0.05	0.13	2.00	0.12	0.05	0.34	0.00	0.05	0.70	0.25	0.45	12	442	11	0.58	459	15	0.60
Silesia 25	3.59	0.41	1.72	0.04	0.23	2.00	0.11	0.01	0.39	0.00	0.03	0.65	0.22	0.43	7	470	13	0.61	444	7	0.58
Ch3	3.69	0.31	1.56	0.12	0.31	2.00	0.10	0.01	0.40	0.00	0.02	0.64	0.21	0.43	5	428	4	0.56	477	16	0.63
Ch4	3.66	0.34	1.60	0.12	0.28	1.99	0.11	0.01	0.38	0.00	0.02	0.64	0.22	0.41	4	462	8	0.61	461	8	0.60
1M4	3.73	0.27	1.57	0.13	0.28	1.98	0.13	0.01	0.33	0.00	0.01	0.60	0.25	0.35	3	504	5	0.66	497	4	0.65
CIC 1/20	3.62	0.38	1.67	0.13	0.20	2.00	0.15	0.02	0.25	0.00	0.02	0.59	0.31	0.28	5	571	7	0.75	546	2	0.72
Mikołów 27	3.74	0.26	1.57	0.14	0.28	1.99	0.15	0.01	0.24	0.00	0.01	0.56	0.30	0.26	3	590	8	0.77	572	5	0.75
1Cz2	3.79	0.21	1.55	0.14	0.31	1.99	0.15	0.01	0.21	0.00	0.01	0.54	0.30	0.24	5	549	−4	0.72	555	−3	0.73
2M2	3.81	0.19	1.55	0.14	0.30	1.98	0.15	0.01	0.21	0.00	0.01	0.53	0.30	0.23	4	602	4	0.79	555	−4	0.73
2M3	3.86	0.14	1.52	0.14	0.32	1.98	0.18	0.01	0.13	0.00	0.01	0.51	0.36	0.14	4	676	5	0.89	625	−3	0.82
1Cz3	3.87	0.13	1.51	0.16	0.32	1.99	0.18	0.01	0.10	0.00	0.00	0.47	0.36	0.11	3	670	0	0.88	637	−5	0.84
2M6	3.90	0.10	1.52	0.15	0.33	1.99	0.18	0.02	0.06	0.00	0.01	0.45	0.37	0.08	7	704	1	0.92	673	−3	0.88
1Cz5	3.90	0.10	1.54	0.14	0.32	2.00	0.20	0.01	0.03	0.00	0.00	0.44	0.39	0.04	0	686	−6	0.90	678	−7	0.89
1Cz4	3.92	0.08	1.51	0.15	0.33	1.99	0.19	0.01	0.02	0.00	0.00	0.42	0.39	0.04	0	714	−3	0.94	712	−3	0.94
Wyoming	3.91	0.09	1.53	0.21	0.24	1.98	0.19	0.01	0.02	0.00	0.00	0.39	0.37	0.02		646	−13	0.85	731	−2	0.96
Cheto	3.98	0.02	1.41	0.08	0.51	2.00	0.24	0.01	0.01	0.01	0.01	0.53	0.49	0.03		846	14	1.11	814	10	1.07
Mean															4						

and Mg. The ammonium content, when analyzed as a percentage of substitution for K, ranges from a few percent to >10% (4% on average), but does not follow a clear trend. A good positive correlation exists for Al^{IV} (R^2 = 0.85). A strong inverse correlation was found between FIX and EXCH:

$$EXCH = -0.43 \times FIX + 0.41 \qquad R^2>0.98 \qquad (1)$$

If the relationship is assumed to be valid for the entire I-S series, then extrapolation to theoretical pure smectite (FIX = 0) gives a smectitic charge of 0.41 and to pure illite (EXCH = 0) gives an illitic charge of 0.95, which is close to mica. Does equation 1 imply that these charges are stable in the entire illite-smectite series? In order to understand the meaning of equation 1, the relationship between FIX and EXCH was analyzed theoretically.

Theoretical analysis of illite-smectite parameters

FIX vs. EXCH. Both the FIX and EXCH values depend on the charge of illite (Q_i) and smectite (Q_s) interlayers, respectively, and the fractions of these interlayers in the I-S structure. Both FIX and EXCH refer to bulk illite-smectite, and thus can be considered as the respective layer charges equally distributed (not in a physical but rather in a mathematical sense, during calculation of the structural formula) over all silicate layers in the mixed-layer clay. If the fraction of smectite interlayers is defined as f_s, then the fraction of illite is $1-f_s$, and the following relations apply:

$$FIX = Q_i \times (1 - f_s) \qquad (2)$$

and

$$EXCH = Q_s \times f_s \qquad (3)$$

FIX and EXCH are parameters of the bulk I-S, and in a mixed-layer crystal of N silicate layers only $N-1$ interlayers exist. Equations 2 and 3 are therefore true only if the external basal surfaces of a crystal are considered as an extra interlayer. This assumption is implicit in all measurements of TSSA, which, since the work of Dyal and Hendricks (1950), is based on the TSSA of smectite, calculated from the unit-cell dimensions and the molecular weight. The nature of the basal surfaces (smectitic or illitic) strongly affects f_s because the value for N of illite-smectite is a small number, commonly the mean of 5 to 12 according to high-resolution transmission electron microscopy (*e.g.* Środoń *et al*., 1990) and XRD (*e.g.* Drits *et al*., 1997c) measurements. However, the smectitic *vs*. illitic nature of the external basal surfaces of the mixed-layer crystals is irrelevant for the considerations outlined below.

Solving the above set of equations leads to the analytical form of the relation between FIX and EXCH, analogous to the experimental regression (equation 1):

$$EXCH = -\,Q_s/Q_i \times FIX + Q_s \qquad (4)$$

The relationship is linear only if Q_s and Q_i are stable. Compared to the experimental regression (equation 1), Q_s = 0.41 and Q_s/Q_i = 0.43, thus Q_i = 0.95. However the slope of this line is the ratio: $-Q_s/Q_i$, instead of a single value, thus the slope can be preserved if the layer charges are variable but their ratio stays constant. Equations 2 and 3 were used to model this alternative, assuming the layer-charge relations from previous studies described in the Introduction, where Q_s increases during the illitization from 0.41 to 0.63 and Q_i from 0.65 to 0.95. The relation between FIX *vs*. EXCH for variable charges is not perfectly linear, but it is close (Figure 4). Based on the available experimental data (Figure 3), the variable-charge case cannot be excluded. The deviation from linearity is apparent only if one charge is set as stable and the other as variable (Figure 4).

Determining whether Q_i and Q_s layer charges are stable or variable is impossible using the structural formulae data alone. However, equations 2 and 3 can be used if an independent measurement of f_s is available. The modeled relations between f_s and FIX and EXCH are linear for constant Q_i and Q_s, and concave or convex for variable values (Figure 5). The techniques for measuring f_s are discussed below.

Independent measurements of f_s. One way to obtain an independent estimate of f_s is from the TSSA, which is the sum of all smectitic surfaces in an I-S structure. Thus:

$$f_s = TSSA/TSSA_{smectite} \qquad (5)$$

$TSSA_{smectite}$, used as a reference in equation 5, should correspond to the same molecular weight as the measured TSSA because TSSA also depends on the molecular weight (equation 5a in Środoń and McCarty, 2008). It is an approximate calculation, ignoring the edge surfaces, but this simplification introduces <4% error (see below).

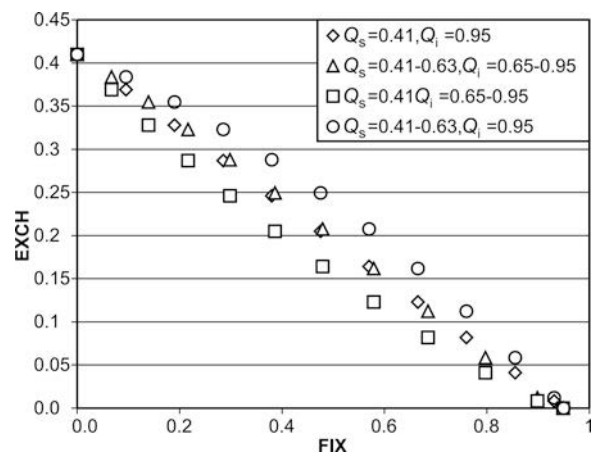

Figure 4. Relations between fixed (FIX) and exchangeable (EXCH) cations per $O_{10}(OH)_2$, modeled using equations 2 and 3 for stable and variable Q_i and Q_s.

https://doi.org/10.1346/CCMN.2009.0570511 Published online by Cambridge University Press

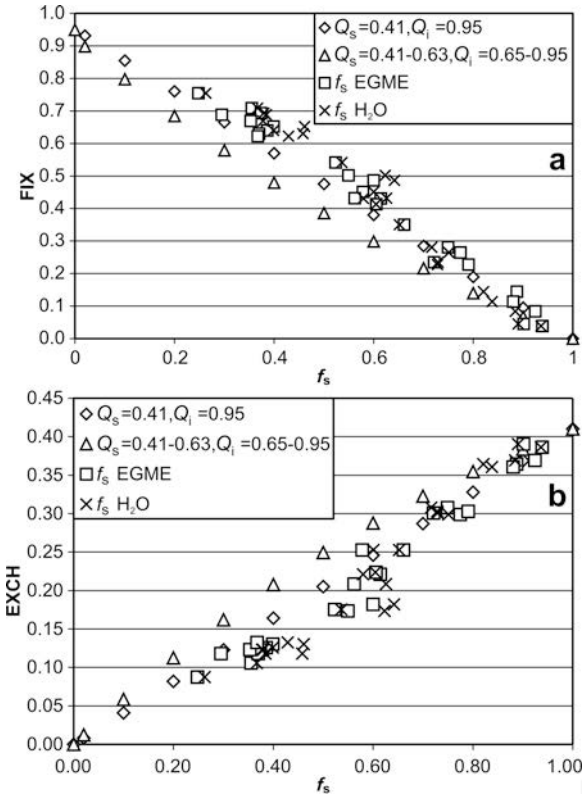

Figure 5. Modeled relationships of FIX and EXCH (calculated for stable and variable Q_i and Q_s) with fraction of expandable layers (f_s). The models were tested using f_s values calculated from H_2O- and EGME-retention data (see text for details).

Equation 5 implies that the end-member illite (f_s = 0) does not have surfaces adsorbing polar molecules responsible for the sample's TSSA. Theoretically, TSSA = 0 either if the external surfaces of a thin illite crystal do not adsorb polar molecules, or the crystal is so thick that the effect of adsorbing surfaces becomes negligible. In nature the latter alternative applies. This conclusion is based on the observation (*e.g.* the data in this paper) of large CEC and TSSA values for R >0 illite-smectites, entirely devoid of smectite monolayers, *i.e.* composed entirely of thin illite fundamental particles (<35%*S* by XRD: *cf.* figure 12 in Środoń *et al.*, 2000).

Another opportunity is offered by the fundamental particle-thickness measurements. A fundamental particle, the term used here *sensu* Nadeau *et al.* (1984), is the finest non-swelling 'building block' of a mixed-layer I-S crystal, *i.e.* a smectite monolayer or a set of illite layers. A simple geometrical analysis (Środoń *et al.*, 1992) indicates that the mean fundamental particle thickness, expressed as the mean number of layers (*N*) of the whole population of illite and smectite layers, is:

$$N = 1/f_s \quad (6)$$

Such f_s is equivalent to $\%S_{MAX}/100$, defined by Środoń *et al.* (1992). Equation 6 is based on the conclusion that all basal surfaces of fundamental particles, including the mixed-layer crystal edges, are smectitic, *i.e.* they hold exchangeable cations and water. The reasoning for this conclusion has been given above (large CEC and TSSA values of samples consisting entirely of illite fundamental particles).

N, if measured (*e.g.* by electron microscopy), can be used to obtain f_s for the tests based on equations 2 and 3. Combining equations 6 and 2 leads to:

$$N = Q_i/(Q_i - \mathrm{FIX}) \quad (7)$$

Being related to equation 6, this formula also relies on the concept of smectitic surfaces of illite crystals. Equation 7 implies that, when FIX approaches Q_i, *N* becomes infinitely large. This explains why clay-sized illites with FIX approaching the end-member value are not available.

The third opportunity to measure f_s is by modeling the X-ray diffraction effects from mixed-layer crystals, as the percentage of smectite layers is one of the key results sought in such modeling (*e.g.* Moore and Reynolds, 1997; Drits *et al.*, 2004).

The approach presented below is based on the TSSA measurements from H_2O and EGME sorption, supported by the CEC data. Problems inherent in the XRD pattern modeling approach are also discussed.

Experimental verification of the model using the TSSA measurements

The TSSA value was calculated from the adsorbed masses (retentions) of water and EGME, using water and EGME coverages (mg/m^2) established from the retention and theoretical surface areas of reference smectites (Środoń and McCarty, 2008). Based on the retention for the most smectitic samples (1Cz5 and 1Cz4: Table 1), the Wyoming sample coverage was used for EGME (0.41 mg/m^2) and intermediate coverage (0.25 mg/m^2) was used for water. The TSSA values calculated by this approach reveal a good linear correlation (Table 3), though they do not extrapolate to 0 for pure illite. f_s was calculated both from H_2O and EGME data using equation 5 (Table 3). The TSSA value of a smectite sample with the same Fe content as a given I-S sample, needed in equation 5, was calculated using the experimental regression of Środoń and McCarty (2008) from the Fe contents (Table 3).

The relationships of the experimental f_s values with FIX and EXCH are similar (Figure 5). For R0 I-S the model of stable Q_i and Q_s is followed. The data deviate from the model, but in the opposite direction from that predicted by the variable Q_i and Q_s model, and for the most illitic samples they fall again on the stable *Q* trend lines.

This type of deviation may indicate that the smectitic coverages given above may not apply to R>0 clays, but that greater values should be used. The greatest deviations in Figure 5 appear to correspond to the

https://doi.org/10.1346/CCMN.2009.0570511 Published online by Cambridge University Press

largest Al^{IV} value in Figure 3, and suggest therefore that the extensive tetrahedral substitution (the layer charge localized over Al-Si substitution sites instead of a random-charge distribution) corresponds to greater values for H_2O and EGME coverage.

The above conclusion was verified using an independent measurement of CEC. Water and EGME retention and CEC correspond to the same surface, thus their ratio should be stable if the liquid coverage and the smectitic layer charge stay constant. Figure 6 presents the ratios of water or EGME retention and CEC_{corr} (values corrected for Ca left on clay after Co-hexamine treatment: see below for details), plotted against FIX, which is used as the measure of the extent of illitization. Both ratios stay constant up to FIX = 0.4, and then both increase significantly. This increase could be due to a smaller smectitic layer charge, which is unlikely, or greater liquid coverage, which is feasible. In the range of stable ratios, the TSSA and f_s values measured from water and EGME retention are reliable, and they support the stable-charge model (Figure 5).

Stable Q_i and Q_s values are the best explanation for the experimental data shown in Figure 3e and this allows use of equations 2, 3, 5, and 7 to calculate f_s, TSSA, and N from structural formulae data. The results are presented below.

Illite-smectite parameters calculated from structural formulae

The f_s values obtained from EXCH (equation 3) and FIX (equation 2) are very close (Table 4), except for sample Małe Ciche, which is characterized by an elevated EXCH value due to its large Ca content, probably the result of incomplete dialysis, because the elevated value is not consistent with the CEC (Table 1). f_s based on FIX is therefore considered to be most reliable and is used in further calculations.

The mean particle thickness, N, calculated from f_s (equation 6), allows estimation of the fundamental particle radius (r), based on the regression of Środoń *et al*. (2000, figure 7):

$$r\left(\frac{7728 - 18368 \times N_i + 10988 \times N_i^2}{\pi}\right)^{0.5} \quad (8)$$

where N_i is the mean number of layers in illite fundamental particles. N_i approaches N for N>2 (table 1 of Środoń *et al.*, 2000), so in this range N can be used in equation 8 as a good approximation of N_i. The r calculated for N = 2 was accepted as representative of the more smectitic samples (Table 4), because r does not vary significantly in this compositional range (Środoń *et al.*, 2000).

Knowing N and r permits calculation of the TSSA that accounts for crystal edges ($TSSA_{Nr}$) from equation 1 of Środoń and McCarty (2008):

$$TSSA_{Nr} = \frac{2000}{\rho_{IS}} \times \left(\frac{1}{N^* t_s} + \frac{1}{r}\right) \quad (9)$$

where ρ_{IS} is the density of dry illite-smectite and t_s is the thickness of the silicate layer which varies from 0.96 nm, the value for fully dehydrated smectite (Środoń and McCarty, 2008), to 0.998 nm, the most common value for illite (Drits *et al.*, 1997a). The mean t_s value ($t_s = 0.96f_s + 0.998(1 - f_s)$) was used, even though the effect of the exact value of t_s on TSSA is negligible. The ρ_{IS} value was calculated from the molecular weight (MW) obtained from the structural formula and the unit-cell parameters based on the unit-cell parameter b obtained from d_{06} and the mean t_s (*cf.* Środoń and McCarty, 2008). The effect of r on TSSA is small, because r is large compared to N; if edges are ignored, *i.e.* r is infinitely large in equation 9, the resulting $TSSA_N$ is only 2−3% smaller (Table 4). The calculation of TSSA by equation 9 is considered most accurate and used as the reference throughout this study.

An alternative calculation of TSSA from f_s is possible *via* equation 5, if the TSSA of pure smectite of the same molecular weight as the investigated sample is known. Such a value for TSSA can be obtained from an experimental regression relating $TSSA_{Nr}$ to the Fe content of smectite (Środoń and McCarty, 2008). The resulting TSSA values (Table 4) are identical to the $TSSA_{Nr}$ values for smectitic samples and are up to 4% greater for illitic samples. This systematic discrepancy reflects the approximate character of the calculation *via* equation 5, which assumes that TSSA corresponds only to basal smectitic surfaces of fundamental particles of I-S and the edge surfaces are ignored. This assumption works well for the smectitic end of the I-S series; but at the illitic end, the contribution of the edge surfaces becomes relatively more important because of fewer basal smectitic surfaces. For this reason the TSSA of I-S is overestimated when calculated using the reference TSSA of smectite. This calculation is useful as it proves that the overestimation of f_s and TSSA for the illitic I-S samples, calculated from EGME and H_2O data (Table 3), is much greater than expected from the approximate character of equation 5. This supports the interpretation presented above.

Illite-smectite parameters calculated from CEC and from water- and EGME-retention

As demonstrated above, water- and EGME-retention are not optimum measurements for calculating TSSA and f_s of I-S, because of the excess retention in R>0 I-S. The CEC is an alternative, because it is directly related to EXCH (Środoń and McCarty, 2008). In order to use CEC measurements for TSSA and f_s calculations, the measured values must be corrected for Ca remaining in the sample after Co-hexamine exchange and for the residual water in the sample after heating at 200ºC

https://doi.org/10.1346/CCMN.2009.0570511 Published online by Cambridge University Press

Table 4. Illite-smectite parameters calculated from structural formulae.

Sample name	f_s from EXCH	f_s from FIX	% diff	N from FIX	r (nm)	b from d_{06} (nm)	V (nm^3)	MW (g/mole)	Density (g/cm^3)	TSSA$_{Nr}$ (m^2/g)	TSSA$_N$ (m^2/g)	%diff from TSSA$_{Nr}$ (%)	TSSA from equation 5 (m^2/g)	%diff from TSSA$_{Nr}$ (%)
Nor 27	0.21	0.21	4	4.86	238	0.9005	0.4636	783.8	2.808	151	148	−2	157	4
Fuzz 6	0.26	0.25	1	3.93	183	0.8992	0.4613	777.8	2.800	188	184	−2	195	4
Swe 151	0.32	0.31	1	3.19	139	0.9005	0.4616	770.8	2.772	234	229	−2	240	2
Swe 162	0.31	0.33	−6	3.06	132	0.8997	0.4606	770.5	2.778	244	239	−2	250	2
Fuzz 5	0.30	0.27	11	3.70	169	0.8981	0.4600	776.5	2.803	200	195	−2	207	4
Swe 81	0.29	0.34	−14	2.98	127	0.8997	0.4604	769.3	2.775	252	246	−2	257	2
Fuzz 9	0.29	0.28	5	3.63	165	0.8984	0.4602	776.6	2.802	203	199	−2	211	4
Fuzz 3	0.30	0.30	2	3.39	151	0.8987	0.4601	774.7	2.796	219	214	−2	226	3
Den 8	0.32	0.34	−6	2.90	122	0.8989	0.4595	770.1	2.783	258	252	−2	264	2
Zukowice 2	0.43	0.43	−1	2.33	88	0.8999	0.4590	769.1	2.782	323	315	−3	329	2
Est 62	0.42	0.47	−10	2.12	76	0.8999	0.4583	770.2	2.791	354	345	−3	360	1
Swe 84	0.44	0.49	−9	2.05	72	0.9008	0.4588	766.0	2.772	369	359	−3	372	1
Małe Ciche 5	0.62	0.53	17	1.90	63	0.8981	0.4555	760.2	2.771	399	388	−3	402	1
Silesia 25	0.54	0.55	−1	1.83	63	0.8992	0.4562	760.1	2.767	416	404	−3	418	1
Ch3	0.51	0.55	−7	1.83	63	0.8999	0.4570	764.5	2.778	413	402	−3	416	1
Ch4	0.55	0.56	−3	1.77	63	0.8997	0.4564	763.9	2.780	427	416	−3	431	1
1M4	0.62	0.63	−2	1.58	63	0.8989	0.4544	761.3	2.782	478	466	−2	481	1
CIC 1/20	0.75	0.70	6	1.42	63	0.8992	0.4533	758.3	2.778	534	522	−2	537	1
Mikołów 27	0.73	0.72	1	1.39	63	0.8992	0.4531	757.8	2.777	547	535	−2	549	0
1Cz2	0.73	0.75	−3	1.33	63	0.8989	0.4523	755.1	2.773	571	560	−2	573	0
2M2	0.74	0.76	−3	1.32	63	0.8984	0.4516	754.4	2.774	577	566	−2	579	0
2M3	0.89	0.85	5	1.18	63	0.8989	0.4506	750.9	2.768	646	635	−2	646	0
1Cz3	0.88	0.88	0	1.14	63	0.8981	0.4492	750.1	2.773	670	658	−2	670	0
2M6	0.90	0.91	−1	1.10	63	0.8987	0.4492	747.0	2.762	697	686	−2	694	0
1Cz5	0.95	0.95	0	1.05	63	0.8978	0.4476	745.1	2.764	728	717	−2	726	0
1Cz4	0.94	0.96	−2	1.04	63	0.8978	0.4475	745.2	2.765	733	722	−2	730	0
Wyoming	0.91	0.98	−7	1.02	63	0.8981	0.4475	746.4	2.770	746	734	−2	741	−1
Cheto	1.21	0.96	25	1.04	63	0.8987	0.4483	743.4	2.754	740	729	−2	737	0

f_s – fraction of smectitic layers, N – mean number of layers in fundamental particles, r mean particle radius, V – unit-cell volume, TSSA$_{Nr}$ and TSSA$_N$ – total specific surface area from equation 5 (see text for details).

(Środoń and McCarty, 2008). The assumption that the trivalent Co-hexamine cation substitutes all exchangeable cations is a good approximation for routine work, but for this more sensitive study, the residual Ca must be considered. The first correction was made by multiplying the measured CEC by $1+f_{CaO}$, where f_{CaO} is the ratio between the residual CaO and the total CaO measured on the Ca-sample; both CaO values corrected for the CaO assigned to apatite (Table 1). This ratio varies between 1 and 6%, but in general increases from 2 to 4% with advancing illitization. This trend suggests that bonding forces for divalent Ca are stronger than for trivalent Co-hexamine cations in some sites, perhaps as a result of local charge concentration (see below). The CEC values corrected in this manner (CEC_{corr} in Table 5) were used in Figure 6.

The excess water correction for CEC is based on the 6 wt.% of molecular water remaining in pure Ca-smectites after heating at 200°C (tables 3 and 4 in Środoń and McCarty, 2008). In more illitic samples, this water is assumed to decrease in proportion to the decreasing smectite content. The CEC is assumed to vary between 0 and 100 meq/100 g and is used in the correction calculation as a measure of smectite content. Thus the second correction (CEC_{corr2} in Table 5) is made by multiplying the CEC_{corr} by $(1 + CEC \times 0.06/100)$.

The CEC measured with Co-hexamine and corrected as shown above was compared with CEC calculated from EXCH using equation 10 of Środoń and McCarty (2008). A linear correlation with $R^2 = 0.99$ and a slight systematic deviation was observed.

Values for TSSA, f_s, and N (*via* equation 6) can be calculated from CEC_{corr2} when Q_s is known. TSSA was calculated (Table 5) using equation 11 of Środoń and McCarty (2008) and f_s by combining equation 3 of the present study with the equation 10 of Środoń and McCarty (2008). For R0 I-S, the results of CEC-based calculations are of similar accuracy to H_2O- and EGME-based calculations (Table 3 and 4), but for R>0 I-S the CEC calculations are more accurate. No systematic difference appears between the f_s values calculated from CEC and from EXCH or FIX (Tables 4, 5).

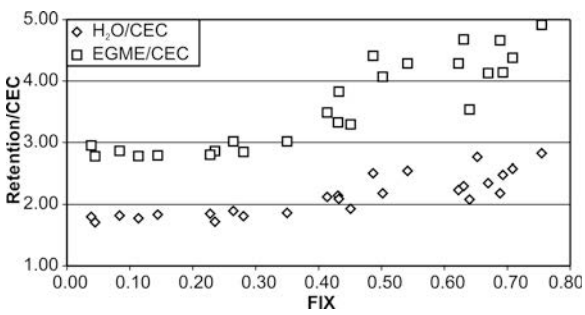

Figure 6. Evolution of the ratios of H_2O and EGME retention (mg/g) to CEC (meq/100 g) in the course of illitization, expressed by the amount of fixed cations (FIX).

The CEC-based calculations of TSSA and f_s, performed above using theoretical formulae, can also be achieved by direct experimental regressions established from the accumulated data (Figure 7). First, CEC_{corr2} is calculated from CEC_{meas} (Figure 7a) and is plotted *vs.* $TSSA_{Nr}$ and f_s from FIX (Figure 7b,c). The results of employing the regressions from Figure 7 are presented in Table 5. The mean relative measurement error is ±4%. Table 5 also shows analogous calculations of TSSA, based on the experimental regression of $TSSA_{Nr}$ (from Table 4) *vs*. water and EGME retention (from Table 1). These regressions are polynomial (Figure 7d,e), and, as expected, the errors of such calculations are greater than if using CEC, especially for R >0 I-S.

XRD determination of % smectite layers and of tridimensional organization

The percentage of smectite layers in I-S ($\%S_{XRD}$) was evaluated by XRD from oriented, glycolated preparations using the peak-position techniques of Środoń (1980; the peaks in the 42−48°2θ region) and of Dudek and Środoń (1996; the peaks in 15−27°2θ region), based on the *NEWMOD* modeling program (Reynolds, 1985), and by whole-pattern modeling using the *SYBILLA* program (Chevron proprietary software), which is a more user-friendly version of the original program by Drits and Sakharov (1976). Both programs allow for detailed modeling of mixed-layered minerals in terms of the nature and the proportions of the layer types and their structural and probability parameters (more details and examples in Drits *et al.*, 1997b; Moore and Reynolds, 1997; Sakharov *et al.*, 1999; Drits *et al.*, 2004; Aplin *et al.*, 2006; McCarty *et al.*, 2008).

In the past, *SYBILLA* and the program by Drits and Sakharov (1976) have mainly been used to qualitatively and quantitatively model multiphase clay assemblages. For this purpose obtaining a close fit between the calculated and the experimental intensities over the entire recorded angular range is necessary. In the current study, however, the purpose was to evaluate the $\%S_{XRD}$ and T (the mean number of 2:1 layers in the mixed-layer crystals) in the predominantly mono-phase I-S samples, which required a different approach and to allow for some simplifications. The 'whole-pattern fitting' (wpf) approach was applied originally, but the result was that the higher-angle reflections and the lower-angle reflections could not be reconciled into one overall satisfactory model but at best into a 'compromise' fit (Figure 8a). Such a fit required an unrealistically large T value (see below) to reasonably match the peak positions of the lower-angle reflections as they were displaced towards smaller angles with decreasing T values, because positions of broader peaks are affected more by the steep LpG^2 at smaller angles (*cf.* Drits *et al.*, 1998). The compromise fit could not model precisely the shape of the 26−27°2θ reflection, which is the illite-

https://doi.org/10.1346/CCMN.2009.0570511 Published online by Cambridge University Press

Table 5. CEC values corrected for Ca left in the clay after Co-hexamine treatment (CEC_{corr}) and for H_2O present in the clay at 200ºC (CEC_{corr2}). Calculation of TSSA and f_s directly from CEC and from regression equations relating $TSSA_{Nr}$ with CEC_{corr2}, H_2O retention and EGME retention.

Sample name	CEC_{corr} (meq/100 g)	CEC_{corr2} (meq/100 g)	TSSA from CEC (m^2/g)	%diff from $TSSA_{Nr}$ (%)	f_s from CEC	%diff from f_s from FIX (%)	TSSA (CEC regr) (m^2/g)	%diff from $TSSA_{Nr}$ (%)	f_s (CEC regr)	%diff from f_s from FIX (%)	TSSA (H_2O regr) (m^2/g)	%diff from $TSSA_{Nr}$ (%)	TSSA (EGME regr) (m^2/g)	%diff from $TSSA_{Nr}$ (%)
Nor 27	17.07	17.25	119	−21	0.16	−20	153	1	0.21	1	148	−2	126	−16
Fuzz 6	26.92	27.35	188	0	0.26	2	219	17	0.29	16	221	18	199	6
Swe 151	28.14	28.61	197	−16	0.27	−14	227	−3	0.30	−3	251	7	273	16
Swe 162	36.17	36.79	253	3	0.35	6	233	−5	0.31	−5	242	−1	223	−9
Fuzz 5	29.45	29.95	205	3	0.28	5	233	16	0.31	15	234	17	209	4
Swe 81	31.38	31.94	219	−13	0.30	−11	242	−4	0.32	−4	230	−8	270	7
Fuzz 9	26.46	26.87	184	−10	0.25	−8	213	5	0.29	4	180	−12	212	4
Fuzz 3	29.40	29.92	205	−6	0.28	−4	238	9	0.32	8	219	0	207	−5
Den 8	32.06	32.64	224	−13	0.31	−11	246	−5	0.3	−5	229	−11	246	−4
Zukowice 2	40.05	41.00	282	−13	0.38	−11	308	−5	0.41	−5	346	7	338	5
Est 62	48.92	50.28	345	−3	0.47	0	351	−1	0.4	−2	366	3	419	18
Swe 84	46.50	47.74	329	−11	0.45	−9	340	−8	0.45	−8	409	11	437	18
Małe Ciche 5	58.42	60.37	413	3	0.56	7	416	4	0.55	4	392	−2	398	0
Silesia 25	55.91	57.71	396	−5	0.53	−2	402	−3	0.53	−3	423	2	379	−9
Ch3	52.23	53.81	370	−11	0.50	−8	380	−8	0.5	−8	377	−9	422	2
Ch4	55.45	57.24	393	−8	0.53	−6	405	−5	0.5	−6	413	−3	401	−6
1M4	68.98	71.71	491	3	0.67	5	485	2	0.64	1	461	−3	447	−6
CIC 1/20	80.38	84.13	577	8	0.78	10	565	6	0.74	5	542	1	515	−4
Mikołów 27	79.40	83.00	569	4	0.77	6	551	1	0.72	0	565	3	552	1
1Cz2	81.43	85.28	584	2	0.79	4	572	0	0.75	0	515	−10	528	−8
2M2	83.02	87.11	596	3	0.80	5	594	3	0.78	2	581	1	527	−9
2M3	93.91	99.14	679	5	0.91	7	667	3	0.87	3	677	5	632	−2
1Cz3	96.17	101.54	695	4	0.93	6	668	0	0.87	−1	669	0	651	−3
2M6	98.56	104.31	714	2	0.95	4	696	0	0.91	0	715	3	709	2
1Cz5	102.47	108.68	743	2	0.99	4	723	−1	0.9	−1	691	−5	717	−2
1Cz4	101.13	107.18	733	0	0.97	2	714	−3	0.9	−3	730	0	774	6
Mean				7		7		4		4		6		7

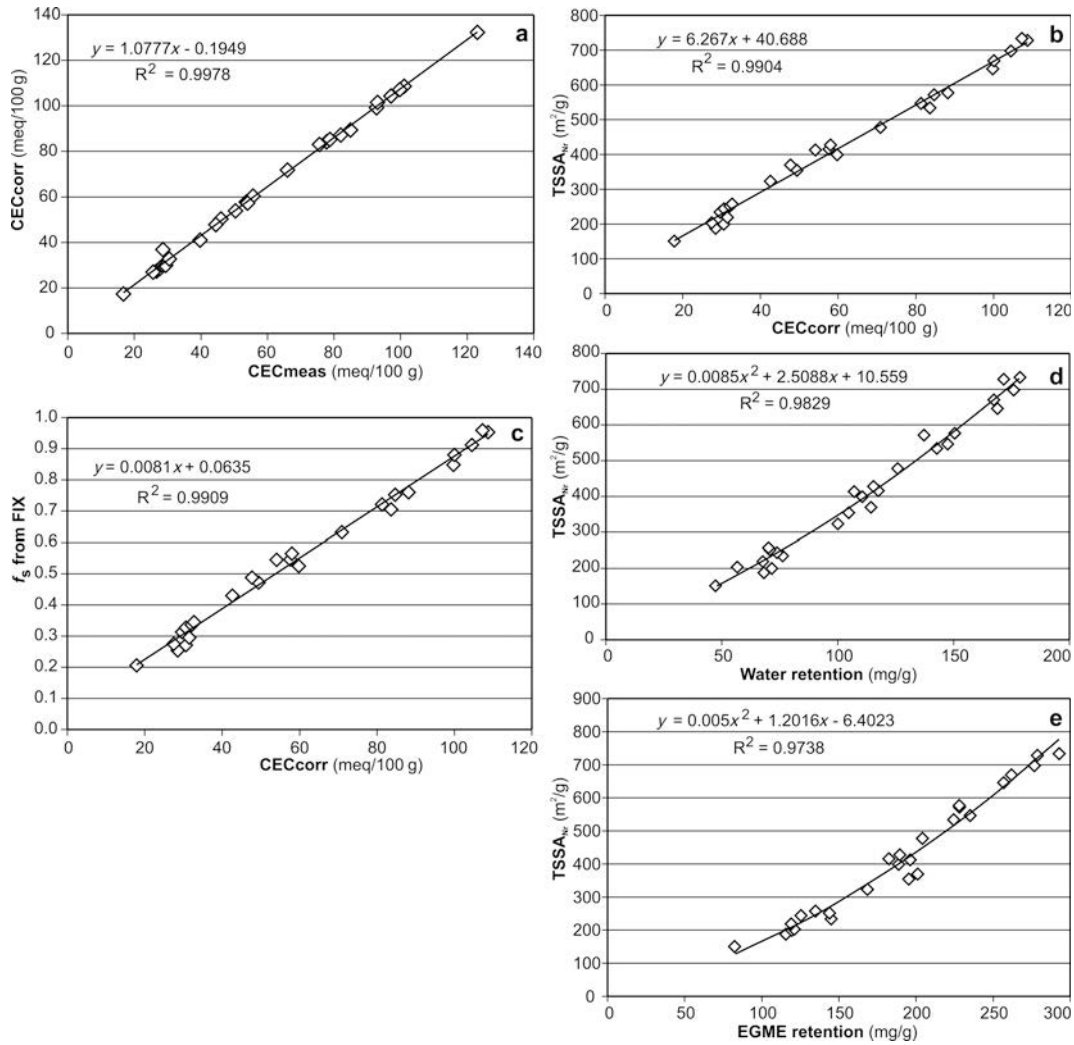

Figure 7. Experimental regressions, based on data from Tables 1, 3, and 4, used to correct measured CEC (a); to calculate $TSSA_{Nr}$ (b) and f_s (c) from such corrected CEC; and to calculate $TSSA_{Nr}$ from water (d) and EGME retention (e).

smectite peak most strongly controlled by *T* (Drits *et al.*, 1997c).

To overcome this problem the shape of the illite-smectite reflection at 26–27°2θ was chosen to model *T* accurately. The precise evaluation of $\%S_{XRD}$ was based on a close fit of peak positions and shapes for all reflections >26°2θ, allowing for a worse fit at smaller angles (Figure 8b). In this approach the most important parameters to be modeled precisely were: $\%S_{XRD}$, *T*, the junction probabilities of R>0 I-S, smectite *d* spacing (d_s) and its fluctuation (δd_s), and illite *d* spacing (d_i) and its fluctuation (δd_i). The last two variables were found to change from the default values 9.98 and 0 only in the case of highly illitic, ammonium-rich samples. Illite layer Fe and K contents and smectite layer Fe, Ca, water, and glycol contents were unchanged from their approximated values in the 'compromise' fit, as they only influence absolute intensities and not peak positions or peak shapes and thus are unimportant in determining $\%S_{XRD}$. For this reason the K content was actually left unchanged from its default value of 0.85 atoms of K per half unit cell. The approximated Fe contents were found to be very close to the Fe contents evident from the structural formulae calculations (on average within 0.08 atoms of Fe per half unit cell). The actual Fe- and K-content values from the structural formulae were used as fixed parameters for a few samples but no measurable differences in output values for $\%S_{XRD}$ and *T* were observed.

Most attention was paid to obtaining a good fit for the glycolated state as the expandable layers were found to exhibit an heterogeneous swelling in the air-dry state. The presence of the tobellite layers was ignored and instead a larger illite *d* spacing was used as compensation when necessary, because the *SYBILLA* program does not support illite-tobellite-smectite mixed-layered struc-

https://doi.org/10.1346/CCMN.2009.0570511 Published online by Cambridge University Press

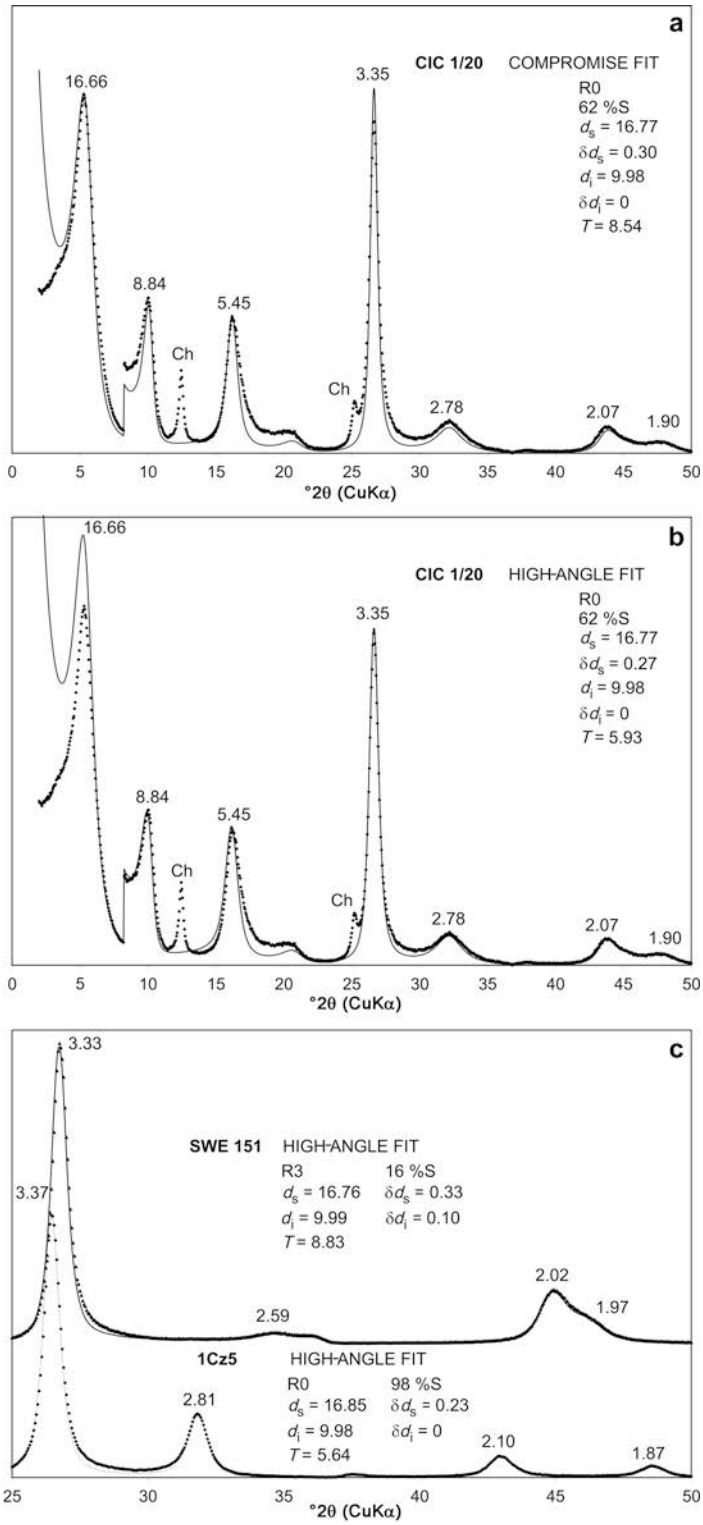

Figure 8. Examples of *SYBILLA* models and experimental XRD patterns of glycolated, Ca^{2+}-saturated I-S. Comparison of two models for sample CIC 1/20 (chlorite peaks not modeled): (a) 'compromise fit' based on the entire angular range; (b) 'high-angle fit' employing peaks >26°2θ c) examples of 'high-angle fits' for samples with different layer compositions. The *d* values for the peaks are shown in Å. Key parameters used in the models are listed in the figures: R (Reichweite), d_s and d_i (smectite and illite layer thicknesses, respectively), δd_s and δd_i (fluctuation of smectite and illite layer thicknesses), and T (mean thickness of the mixed-layer crystals). In (a) and (b) the scale of the patterns is increased $\times 4$ at 8.25°2θ for clearer presentation.

https://doi.org/10.1346/CCMN.2009.0570511 Published online by Cambridge University Press

tures for R >1 (and samples with R>1 are those with the most NH_4^+ content). Given the relatively small contribution of tobellite layers (4% of FIX on average), the impact of this simplification on the $\%S_{XRD}$ determined is negligible. Furthermore, it was decided to use only two layer types (illite and smectite) to model the patterns, as initial trials showed that the use of a third layer type (vermiculite) had a very limited impact on improving the fits (very small percentages of this component) and only complicated the modeling process, especially for R>0 structures. The modeled total percentage of expandable layers did not change substantially. The results from Inoue *et al.* (2005), obtained for hydrothermally altered volcanics, and from Lindgreen *et al.* (2000) for shales, also show that in glycolated Ca^{2+} samples, such vermiculitic layers, if present, occur only in small quantities (0–5%). Finally, satisfactory fit could also be obtained using just one I-S phase.

Table 6 lists the results of the *NEWMOD*- and *SYBILLA*-based analyses. Figure 8 compares, for sample CIC 1/20, the compromise fit (a) to the fit based on the larger-angle reflections (b). For all samples, two such fits were modeled and compared. The differences in $\%S_{XRD}$ were generally found to be 2% absolute or less, indicating that this number is very robust (Table 6). The differences in all other parameters used were also small, except for a substantial difference in T (Table 6). *SYBILLA* fits obtained by the large-angle fitting approach are shown (Figure 8c) for a very smectitic sample (1Cz5) and a very illitic sample (Swe 151).

The tridimensional structure of the investigated set of samples evolves with illitization (Figure 2). Down to $50\%S_{XRD}$, the XRD characteristics are essentially turbostratic. At $\sim30\%S_{XRD}$, the beginning of 1*M* organization, both in *tv* (Ch3) and *cv* (Ch4) versions, becomes visible. At $\sim15\%S_{XRD}$, 1*Mtv* (Fuzz 9), 1*Mcv* (Swe 162), and 1*Md* (Den 8) polytypic varieties were observed. The evolution in the 36–38º2θ range indicates that $n \times 120^o$ rotations are dominant (*cf.* Moore and Reynolds, 1997).

f_s compared to $\%S_{XRD}$

Plots of f_s (from Table 4) *vs.* $\%S_{XRD}$ data sets from Table 6 (Figure 9) are very similar: in most cases XRD underestimates the smectite layer content calculated from chemistry (f_s), with the largest differences at intermediate and small values for f_s. The underestimation is greatest for measurements based on the peaks in the 15–27º2θ region, intermediate for the peaks in 42–48º2θ region, and smallest for the *SYBILLA* models.

The general shape of the plot in Figure 9 can be attributed to the effect of the small thickness of illite-smectite crystals: computer models do not account for the external surfaces of illite-smectite crystals. Assuming that these surfaces are smectitic, it follows that the XRD measurements underestimate the smectite content (Środoń *et al.*, 1992), and that this underestimation should be greatest for the most illitic compositions (*cf.* Środoń, 1999). On the other hand, if the mixed-layer crystal edges were illitic (at least those edges which have the neighboring illitic interlayer), then for illite no difference would be observed between the XRD estimate and f_s, and for more smectitic compositions the XRD numbers would be close to f_s. This reasoning does not rely on the fundamental particle concept but just on the properties of the mixed-layer crystals (Figure 10). It follows that the data presented in Figure 9 can be considered as proof of the smectitic nature of mixed-layer crystal edges.

In order to verify the conclusion above quantitatively, the experimental relationship between the mean number of layers in the fundamental particles (N) and in the mixed-layer crystals (T) was established using wholly independent data: N measured by TEM (Środoń *et al.*, 2000) and T measured by the modified Scherrer equation (Drits *et al.*, 1997c) and by the Bertaut-Warren-Averbach technique (Drits *et al.*, 1998):

$$T = 0.763 \times N + 4.113 \quad R^2 = 0.89 \qquad (10)$$

Then N values from Table 4 were used to calculate T (referred to as 'T from equation 10' in Table 7), and from these two values the theoretical value of $\%S_{XRD}$ ($\%S_{XRD\ theor}$) was calculated applying the smectitic crystal-edge assumption (equation 9 of Środoń *et al.*, 1992) and plotted in Figure 9 *vs.* f_s from Table 4. The plot demonstrates that most of the underestimation has been explained. In the intermediate range of f_s, the $\%S_{XRD}$ is even smaller than expected from the model. This discrepancy deserves further study. Equation 10 gave T values quite close to the values modeled in *SYBILLA* by the large-angle fitting approach (compare T from equation 10 in Table 7 with T (haf) in Table 6).

Equation 9 of Środoń *et al.* (1992) was also applied differently to calculate T using N from Table 4 and $\%S_{XRD}$ from Table 6. Considering how sensitive this calculation is to small errors in $\%S_{XRD}$ (especially for

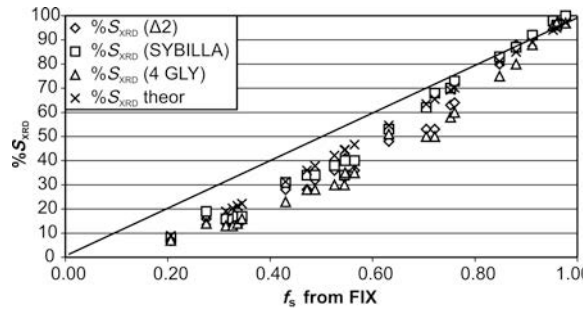

Figure 9. Fraction of smectitic layers (f_s) calculated from FIX *vs.* percent expandable layers measured by two XRD peak-position techniques and by *SYBILLA* modeling (from Table 6). This relationship is modeled using theoretical $\%S_{XRD}$ values calculated by rearranged equation 10 of Środoń *et al.* (1992) from the thickness of the fundamental particles (N in Table 4) and of the mixed-layer crystals (T in Table 6).

https://doi.org/10.1346/CCMN.2009.0570511 Published online by Cambridge University Press

Table 6. XRD data from oriented preparations (columns 1–11). Mixed-layer peaks are identified by number and type of treatment (air-dry *vs.* ethylene glycol). Expandibility calculations by the peak-position method of Dudek and Środoń (1996, column 12), Δ2 method of Środoń (1980, column 13), and *SYBILLA* modeling (column 14: whole-pattern fitting; column 15: high-angle fitting (haf)). Columns 16 and 17 compare mean number of layers in mixed-layer crystals (*T*) used in wpf and haf modeling. Columns 18–22 provide parameters used in *SYBILLA* haf modeling: Reichweite (R), glycol smectite layer thickness (d_s) and its mean fluctuation (δd_s), illite layer thickness (d_i) and its mean fluctuation (δd_i).

Sample	2 AIR	1 GLY	2 GLY	3 GLY	4 GLY	5 GLY	6 GLY	7 GLY	8 GLY	Δ2=8GLY-7GLY	%*S* (4/5)	%*S* (Δ2)	%*S* (wpf)	%*S* (haf)	*T* (wpf)	*T* (haf)	R	d_s	δd_s	d_i	δd_i
Column no.	1 (°2θ)	2 (°2θ)	3 (°2θ)	4 (°2θ)	6 (°2θ)	7 (°2θ)	8 (°2θ)	9 (°2θ)	10 (°2θ)	11=10-9 (°2θ)	12	13	14	15	16	17	18	19 (Å)	20 (Å)	21 (Å)	22 (Å)
Nor 27	8.55		8.28	8.92	17.58	26.76	35.22	45.26			7		8	8	11.12	10.57	R3	16.77	0.29	9.98	0.10
Swe 151	8.20		7.75	9.20	17.30	26.75	34.65	44.95	46.15	1.20	13	14	16	16	10.28	8.83	R3	16.76	0.33	9.99	0.10
Swe 162	8.10		7.75	9.25	17.25	26.70	34.65	44.80	46.25	1.45	13	16	16	16	9.99	8.54	R3	16.80	0.30	10.00	
Swe 81	8.10		7.65	9.15	17.20	26.65	34.55	44.70	46.15	1.45	14	16	17	16	9.70	8.54	R3	16.82	0.28	10.01	0.10
Fuzz 9	8.10		7.80	9.25	17.20	26.65	34.70	44.75	46.20	1.45	14	16	19	19	10.28	10.28	R3	16.79	0.32	10.00	
Den 8	8.15		7.46	9.16	17.08	26.62	34.42	44.62	46.00	1.38	16	15	17	18	9.23	8.25	R3	16.79	0.29	10.03	0.10
Zukowice 2	7.70	2.60	6.95	9.50	17.00	26.80	34.00	44.60	47.00	2.40	23	28	31	31	9.41	6.51	R2	16.70	0.34	9.98	
Est 62	7.45	2.55	6.85	9.45	16.85	26.75	33.80	44.50	46.90	2.40	28	28	34	34	9.41	5.93	R2	16.74	0.34	9.98	
Swe 84	7.50	2.65	6.75	9.50	16.85	26.75	33.80	44.40	47.10	2.70	28	32	34	35	9.99	5.64	R2	16.77	0.32	9.98	
Małe Ciche 5	7.45	2.90	6.75	9.65	16.75	26.70	33.75	44.25	47.20	2.95	30	36	38	40	7.09	7.09	R2	16.70	0.30	10.02	
Silesia 25	7.30	3.15	6.70	9.70	16.70	26.65	33.55	44.15	47.35	3.20	35	41	40	42	8.83	6.80	R2	16.74	0.22	9.98	
Ch3	7.50	2.95	6.75	9.60	16.75	26.70	33.65	44.30	47.05	2.75	30	33	36	38	9.12	6.22	R2 (R1)	16.78	0.32	9.98	
Ch4	7.45	3.00	6.60	9.75	16.70	26.70	33.50	44.20	47.15	2.95	35	36	40	41	9.70	6.80	R1	16.78	0.25	9.98	
1M4	7.10	3.15	5.90	9.90	16.40	26.60	33.10	43.90	47.40	3.50	51	48	53	56	8.54	6.51	R1	16.80	0.30	9.98	
CIC 1/20	6.45		5.30	10.00	16.25	26.60	32.15	43.80	47.80	4.00	50	53	62	62	8.54	5.93	R0	16.77	0.27	9.98	
Mikołów 27	6.20		5.35	10.00	16.25	26.60	31.90	43.70	47.70	4.00	50	53	68	67	7.09	5.06	R0	16.79	0.32	9.98	
1Cz2	6.35		5.35	10.02	16.20	26.65	32.05	43.55	48.15	4.60	58	63	70	71	7.96	5.93	R0	16.77	0.23	9.98	
2M2	6.20		5.30	10.15	16.10	26.55	31.90	43.50	48.15	4.65	60	64	73	73	9.70	5.64	R0	16.80	0.25	9.98	
2M3	6.15		5.25	10.30	15.95	26.50	31.85	43.20	48.35	5.15	75	80	83	84	9.41	5.64	R0	16.83	0.24	9.98	
1Cz3	6.15		5.25	10.35	15.90	26.50	31.85	43.10	48.45	5.35	80	88	87	88	8.04	5.93	R0	16.83	0.22	9.98	
2M6	6.10		5.20	10.35	15.85	26.50	31.80	43.05	48.50	5.45	88	92	92	93	6.80	5.06	R0	16.83	0.24	9.98	
1Cz5	5.90		5.20	10.40	15.78	26.44	31.84	42.98	48.58	5.60	96	98	98	98	7.09	5.64	R0	16.85	0.23	9.98	
1Cz4	5.90		5.24	10.40	15.82	26.50	31.82	42.98	48.58	5.60	97	98	100	99	7.38	5.06	R0	16.75	0.23	9.98	
Wyoming	6.10		5.20	10.38	15.72	26.34	31.72	42.72	48.40	5.68	97	100	96	96	7.38	5.64	R0	16.83	0.24	9.98	
Cheto	5.85		5.25	10.45	15.85	26.60	31.95	43.10	48.85	5.75	99	100	100	100	5.35	4.19	R0	16.74	0.24	9.98	

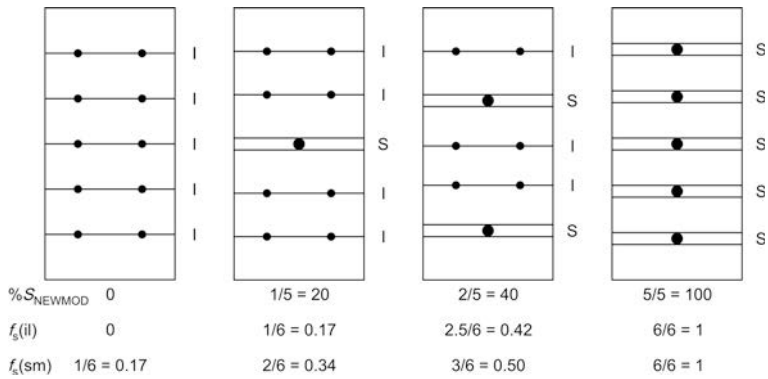

Figure 10. Calculation of layer compositions of illite-smectite mixed-layer crystals under different assumptions about the nature of crystal basal surfaces. %S_{NEWMOD} – surfaces ignored; f_s (il) – illitic or smectitic surface, depending on the nature of the closest interlayer; f_s (sm) – surfaces always smectitic. %S_{NEWMOD} *vs.* f_s (sm) model explains the data presented in Figure 9.

large %S_{XRD} values), in the reliable, highly illitic range, the results are consistent with the calculations based on equation 10 (Table 7).

The small but systematic differences between the measurements of %S_{XRD} are understandable artifacts of the modeling techniques. The *NEWMOD* computer program does not account for external crystal surfaces, and thus strongly underestimates %S_{XRD}, as I-S crystals are very thin (Środoń *et al.*, 1990, 1992). The algorithms of Drits and Sakharov (1976) include one crystal edge in the calculation, treating it either as smectitic or illitic; thus they also underestimate the smectite content, but to a lesser extent. This difference in models can explain why %S_{XRD} values from *SYBILLA* are generally greater than those from *NEWMOD*-based techniques.

The difference between the two *NEWMOD*-based techniques can be traced to the use of the 15.5–17.5º2θ reflection in one of them. This peak, when modeled, is quite asymmetric, while in the experimental patterns it is much more symmetric (Figure 8). The strong asymmetry of the modeled reflection is interpreted here as being the result of a simplified structural factor function selected for the model (*cf.* discussion by Drits *et al.*, 1998, concerning the illite 001 peak). Perhaps such simplification can displace the maximum of the peak toward lower angles from the position of the interference function. Judging from the more symmetric peaks of the experimental patterns, in natural samples this effect is much smaller due to the natural chemical heterogeneity of I-S, resulting in variability of the structure factors. As a result, for a given %S_{XRD}, the peak position of a natural sample is displaced toward a more illitic composition with respect to the modeled peak, which was used for the calibration. This effect of the use of simplified structure factors by the computer models forced us to use the high-angle fitting approach, as it is displacing peak maxima in 001 and 002 illite ranges.

The selected XRD peak positions from Table 6 were plotted *vs.* f_s from Table 4 (Figure 11). If the angular distance between end-member reflections of illite and smectite is <2.5º2θ, the corresponding mixed-reflection positions or their angular distance (Δ2) are related to f_s by linear equations (Figure 11a,c,e,f). For more distant end-member reflections, this relationship was more complex (Figure 11b,d). The experimental regressions (Figure 11) can be used for measuring f_s from the XRD data. The regressions in Figure 11b,d are applicable only to R>0 I-S (*cf.* Środoń, 1984). Calculations of f_s using the experimental regressions are presented in Table 7. The errors are random, thus averaging results produces the most accurate numbers. Sample Fuzz 9 gives the largest error, probably due to the crystal-size effect. This is the only hydrothermal sample in the set and its crystal size is much larger (Table 6).

The linear regressions in Figure 11 extrapolate to positions characterizing discrete end-member illite (9.98 Å) not at f_s = 0 but at ~0.10–0.15, equivalent to N = 7–10 (equation 6). This seems to indicate that beginning from this level of N, illite fundamental particles exist independently, *i.e.* their tendency to associate into mixed-layer crystals disappears ($N = T$), and all exchange cations still present in such clays come from the external surfaces of illite crystals.

Chemical composition of the end-member minerals

The trends from Figure 3, when extrapolated to FIX = 0.95, yield an average composition of end-member illite close to intermediate between muscovite and phengite:

$$FIX_{0.95}(Si_{3.25}Al_{0.75}))(Al_{1.81}Fe_{0.01}Mg_{0.19})O_{10}(OH)_2$$

The end-member smectite composition obtained by extrapolation to FIX = 0 is a montmorillonite intermediate between Wyoming and Cheto:

$$EXCH_{0.41}(Si_{3.95}Al_{0.05}))(Al_{1.48}Fe_{0.17}Mg_{0.35})O_{10}(OH)_2$$

The interlayer and the tetrahedral sheet compositions in these formulae are more reliable than the octahedral-sheet composition, the latter extrapolated from data which are quite scattered (Figure 3). Such scatter was attributed by Ylagan *et al.* (2000) and Inoue *et al.* (2004) to the chemical composition of the reacting solutions.

https://doi.org/10.1346/CCMN.2009.0570511 Published online by Cambridge University Press

Table 7. Mean thickness of the mixed-layer crystals (T) calculated by different techniques (see text for details) and fractions of smectitic layers (f_s) calculated from experimental regressions (Figure 10).

	T (from equation 10)	T (from %S *SYBILLA*)	T (from %S Δ2)	f_s (2 GLY)	%diff from f_s (FIX)	f_s (3 GLY)	%diff from f_s (FIX)	f_s (4 GLY)	%diff from f_s (FIX)	f_s (6 GLY)	%diff from f_s (FIX)	f_s (7 GLY)	%diff from f_s (FIX)	f_s (Δ2)	%diff from f_s (FIX)	f_s (mean)	%diff from f_s (FIX)
Nor 27	7.82	7.31	6.85	0.19	−9	0.17	−15	0.17	−18	0.16	−22	0.19	−9			0.18	−15
Swe 151	6.55	5.48	4.96	0.30	−5	0.32	1	0.29	−8	0.29	−6	0.29	−8	0.29	−9	0.30	−6
Swe 162	6.45	5.04	5.04	0.30	−9	0.34	5	0.31	−5	0.29	−10	0.34	4	0.32	−1	0.33	−3
Swe 81	6.38	5.00	4.77	0.32	−5	0.29	−13	0.33	−2	0.32	−6	0.37	11	0.32	−4	0.33	−3
Fuzz 9	6.89	9.50	7.29	0.29	4	0.34	24	0.33	20	0.28	2	0.36	29	0.32	17	0.34	16
Den 8	6.33	4.75	4.36	0.36	4	0.30	−14	0.38	11	0.35	1	0.40	16	0.31	−10	0.35	1
Zukowice 2	5.89	5.75	4.80	0.46	8	0.47	9	0.42	−3	0.44	3	0.41	−6	0.46	8	0.44	3
Est 62	5.73	5.01	3.75	0.48	3	0.44	−6	0.48	2	0.49	4	0.44	−7	0.46	−2	0.46	−1
Swe 84	5.68	4.47	4.05	0.51	4	0.47	−4	0.48	−1	0.49	1	0.47	−3	0.51	4	0.48	0
Małe Ciche 5	5.57	4.26	3.87	0.51	−4	0.55	4	0.52	0	0.50	−4	0.52	−1	0.54	3	0.53	0
Silesia 25	5.51	4.10	4.33	0.52	−6	0.57	5	0.55	0	0.55	0	0.56	2	0.58	6	0.56	1
Ch3	5.51	3.22	3.11	0.51	−7	0.52	−5	0.52	−4	0.53	−4	0.51	−7	0.51	−6	0.52	−5
Ch4	5.47	3.64	3.13	0.54	−5	0.60	6	0.55	−3	0.5	−1	0.54	−5	0.54	−4	0.56	−2
1M4	5.32	4.62	3.43			0.67	7	0.67	7			0.64	1	0.62	−1	0.65	3
CIC 1/20	5.20	4.49	2.69			0.72	3	0.74	5			0.67	−5	0.70	−1	0.71	0
Mikołów 27	5.17	7.72	2.45			0.72	0	0.74	2			0.70	−2	0.70	−3	0.72	−1
1Cz2	5.13	5.73	3.02			0.73	−2	0.76	1			0.75	0	0.79	5	0.76	1
2M2	5.12	8.93	2.99			0.80	5	0.80	6			0.77	1	0.79	4	0.79	4
2M3	5.01	9.32	4.15			0.88	3	0.87	2			0.87	3	0.87	2	0.87	3
1Cz3	4.98	12.47	281.05			0.90	2	0.89	1			0.90	3	0.90	2	0.90	2
2M6	4.95	−10.08	−10.08			0.90	−1	0.91	0			0.92	1	0.91	0	0.91	0
1Cz5	4.91	−0.73	−0.73			0.93	−3	0.94	−1			0.94	−1	0.93	−2	0.94	−2
Cheto	4.91	−77.75	−0.97			0.93	−3	0.9	−4			0.94	−2	0.93	−3	0.9	−3
1Cz4	4.89	0.00	0.00			0.92	−6	0.96	−1			1.03	5	0.95	−3	0.96	−1
Wyoming	4.90	0.00	0.00			0.95	−1	0.91	−6			0.90	−6	0.96	−1	0.93	−4

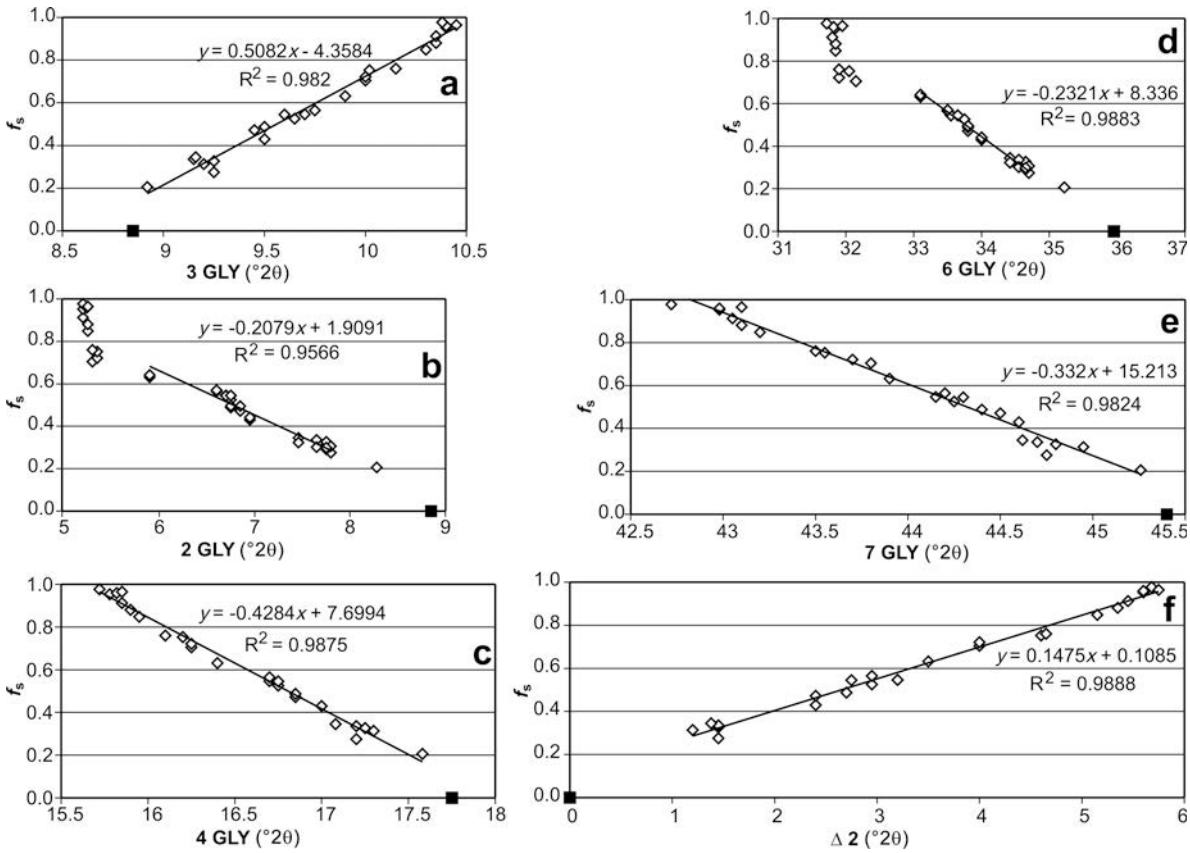

Figure 11. Plots of selected XRD peak positions or angular distances between selected peaks (data from Table 6) *vs.* f_s from Table 4. These experimental regressions can be used for measuring f_s from the XRD data. The theoretical positions of end-member illite reflections (d_{001} = 9.98 Å) are marked by squares.

SUMMARY AND CONCLUSIONS

The major result of this study, *i.e.* evidence of the stability of the charge of illite and smectite layers in the course of illitization, confirms the results of Środoń *et al.* (1992) and Ylagan *et al.* (2000). The evaluation of the smectitic charge is very similar in all three papers. The recognition of an illitic charge so close to that of mica is the result of accounting for fixed ammonium, which was not analyzed in the previous studies, and of the application of the FIX *vs*. EXCH plot instead of plotting FIX *vs.* electron microscopy-based data. If these new results are accepted, several consequences are apparent.

From a general perspective the most important conclusion is that illite is a mineral species closer to mica than previously thought, with a composition intermediate between muscovite and phengite: 95% of the fixed cation positions are occupied. The external surfaces of illite fundamental particles have smectitic charges and hold exchangeable hydrated cations and tightly bound water molecules, which can be expelled only by heating to temperatures of >200ºC. The distinction between illite and I-S could be based on the fundamental particle thickness: at N = 7–10 their tendency to associate into mixed-layer crystals seems to disappear ($N = T$; XRD peak positions correspond to pure illite).

More specific conclusions are:

(1) FIX can be used to calculate all essential parameters of I-S (equations 5, 6, 7, 9, 10).

(2) The CEC can be used also to calculate these parameters *via* experimental regressions (Figure 7). In the case of I-S, the evaluation of TSSA from CEC is more accurate than from H_2O or EGME retention (unlike pure smectites: Środoń and McCarty, 2008).

(3) XRD expandability measurements based on peak-position techniques or modeled by *SYBILLA* are close to each other. Minor systematic differences between these measurements have been detected and explained. They all heavily underestimate f_s (Figure 9); a feature attributed to the limited thickness of the mixed-layer crystals, the smectitic nature of their external surfaces, and the definition of expandability in the models of the diffraction effects. However, the correct f_s values can be measured quite accurately from peak-position data *via* experimental regressions (Figure 11), and all other parameters can be calculated from f_s (equations 5, 6, 9, 10).

https://doi.org/10.1346/CCMN.2009.0570511 Published online by Cambridge University Press

(4) Illite interlayers seem to contain insufficient vacancies to accommodate molecular water released by illites on heating to >300ºC, as assumed by Slonimskaya *et al.* (1978), Loucks (1991), and Drits and McCarty (2007). Środoń and McCarty (2008) demonstrated that pure smectites, devoid of any contracted layers, contain stable amounts of tightly bound water molecules, corresponding to ~1.3% of the mass of dry smectite. The illites studied by Slonimskaya *et al.* (1978) and Drits and McCarty (2007) have FIX = 0.74; thus f_s = 0.22 (equation 7) and N = 4.52 (equation 6). Such an amount of smectitic surface corresponds to ~0.29% of tightly bound H_2O, close to the 0.35−0.37% measured by Drits and McCarty (2007). According to the results of this study, such illite can have a maximum of 0.05 vacancies/ $O_{10}(OH)_2$, which could accommodate up to only 0.18% H_2O. Thus, at least half of the measured, tightly bound water must come from the external, smectitic surfaces of illite crystals. This interpretation explains why the high-temperature dehydration is so easily reversible, as demonstrated by Drits and McCarty (2007) for illites, and by Środoń and McCarty (2008) for smectites.

(5) A stable charge of smectitic layers is an intriguing finding, given a broad charge variability of pure smectites. Either these data support the claim of Sato *et al.* (1996) that smectites evolve chemically before the onset of illitization, or they reflect the restricted chemical composition of parent pyroclastic materials of bentonites (acidic glasses). This alternative deserves further investigation, crucial for the application of a 0.41 smectitic charge to I-S of different origins. Despite its stable charge, the smectitic interlayer properties are evolving, as demonstrated by the greater coverages of H_2O and EGME, as well as the more strongly held Ca in more illitic samples. Such features probably reflect an increasing share of tetrahedral substitution in smectitic charges and changes in charge distribution. Smectitic charge is delocalized and occurs as a 'charge field' provided by a distant octahedral substitution, with exchangeable cations distributed at equal distances one from each other. Tetrahedral substitution provides the charge sites located over the Al-Si substitution sites. In the case of Ca saturation of the tetrahedral-dominated surface layer charge, the divalent cation cannot simultaneously satisfy two strong monovalent negative charge sites which are located at a distance from each other. This provides excess positive charge in one spot and excess negative charge in another. Water is needed, therefore, to distribute charge among charge-saturated/ undersaturated spots. This mechanism can make water adsorption in illitic phases different from that in smectitic I-S. Under the experimental conditions of the present study (Ca^{2+}, ethylene glycol, 47% RH), this evolution did not result in the evolving XRD characteristics (from smectitic to vermiculitic).

The present study resulted in an improved technique for measuring TSSA and CEC values. The technique applied which uses sequential H_2O and EGME sorption and CEC measurement has the advantage of using only one sample split, and of referring all measurements to the same sample weight at 200ºC, which limits the errors related to weighing and to the tightly bound water content. The Co-hexamine technique of Bardon *et al.* (1983) requires correction for Ca^{2+} not exchanged by this procedure, the amount of which increases for more illitic minerals (Table 1).

The study confirmed earlier reports of ammonium in I-S from bentonites (Nadeau and Bain, 1986; Środoń *et al.*, 2006b). On average 4% of ammonium in the fixed cations population (up to 12%) was measured. As bentonite layers have no source of ammonium ions (in contrast to shales), such fixed ammonium represents a record of ammonium migration throughout the rocks, a phenomenon directly related to oil and gas generation.

It should be stressed that the findings of this paper result from studying altered pyroclastics, a specific rock type, offering the opportunity to separate mono-mineral illite-smectite. Further studies will verify if these characteristics apply to illite-smectite in common sedimentary rocks.

ACKNOWLEDGMENTS

This study was financed by research grant no. 2 P04D 078 29 of the Polish Ministry of Science and Higher Education. Mrs Dorota Bakowska and Mrs Małgorzata Zielińska are thanked for careful laboratory work, Dr Tadeusz Kawiak for XRD work, Dr Michał Skiba for providing the FTIR spectra, and Dr Leszek Chudzikiewicz and Dr Andrzej Łaptaś for help with the figures. Chevron ETC and Douglas McCarty personally are acknowledged for permission to use the proprietary *SYBILLA* software and for the XRD measurements of the heated slides under N_2-atmosphere. Douglas McCarty also improved the English of the manuscript. JS acknowledges the financial support of the Université Louis Pasteur, Strasbourg, where the first draft of this paper was written. EZ worked within the framework of his PhD program, financed by The Institute for the Promotion of Innovation through Science and Technology in Flanders (IWT-Vlaanderen). Comments by Atsuyuki Inoue and an anonymous reviewer helped to clarify the presentation of results.

REFERENCES

Aplin, A.C., Matenaar, I.F., McCarty, D.K., and van Der Pluijm, B.A. (2006) Influence of mechanical compaction and clay mineral diagenesis on the microfabric and pore-scale properties of deep-water Gulf of Mexico Mudstones. *Clays and Clay Minerals*, **54**, 500−514.

Bardon, C., Bieber, M.T., Cuiec, L., Jacquin, C., Courbot, A., Deneuville, G., Simon, J.M., Voirin, J.M., Espy, M., Nectoux, A., and Pellerin, A. (1983) Recommandations pour la détermination expérimentale de la capacité d'échange de cations des milieux argileux. *Revue de l'Institut Francais du Pétrole*, **38,** 621−626.

Bergström, S.M., Huff, W.D., Kolata, D.R., and Bauert, H. (1995) Nomenclature, stratigraphy, chemical fingerprinting, and areal distribution of some Middle Ordovician K-bentonites in Baltoscandia. *Geologiska Föreningens i*

https://doi.org/10.1346/CCMN.2009.0570511 Published online by Cambridge University Press

Stockholm Förhandlingar, **117**, 1–13.
Brown, G. and Weir, A.H. (1963) The identity of rectorite and allevardite. *Proceedings of the 1st International Clay Conference*, Stockholm, 1963, vol. **1**, 27–37.
Burchill, P. and Welch, L.S. (1989) Variation of nitrogen content and functionality with rank for some UK bituminous coals. *Fuel*, **68**, 100–104.
Cetin, K. and Huff, W.D. (1995) Layer charge of the expandable component of illite/smectite in K-bentonite as determined by alkylammonium ion exchange. *Clays and Clay Minerals*, **43**, 150–158.
Clauer, N., Środoń, J., Franců, J., and Šucha, V. (1997) K-Ar dating of illite fundamental particles separated from illite-smectite. *Clay Minerals*, **32**, 181–196.
Drits, V.A. and McCarty, D.K. (2007) The nature of structure-bonded H_2O in illite and leucophyllite from dehydratation and dehydroxylation experiments. *Clays and Clay Minerals*, **55**, 45–58.
Drits, V.A. and Sakharov, B.A. (1976) *X-ray Structural Analysis of Mixed-Layer Minerals.* Nauka, Moscow (in Russian).
Drits, V.A., Lindgreen, H., and Salyn, A.L. (1997a) Determination of the content and distribution of fixed ammonium in illite-smectite by X-ray diffraction: Application to North Sea illite-smectite. *American Mineralogist*, **82**, 79–87.
Drits, V.A., Sakharov, B.A., Lindgreen, H., and Salyn, A.L. (1997b) Sequential structure transformation of illite-smectite-vermiculite during diagenesis of Upper Jurassic shales from the North Sea and Denmark. *Clay Minerals*, **32**, 351–371.
Drits, V.A., Środoń, J., and Eberl, D.D. (1997c) XRD measurement of mean crystallite thickness of illite and illite/smectite: reappraisal of the Kubler index and the Scherrer equation. *Clays and Clay Minerals*, **45**, 461–475.
Drits, V., Eberl, D.D., and Środoń, J. (1998) XRD measurement of mean thickness, thickness distribution and strain for illite and illite/smectite crystallites by the Bertaut-Warren-Averbach technique. *Clays and Clay Minerals*, **46**, 38–50.
Drits, V.A., Lindgreen, H., Sakharov, B.A., Jakobsen, H.J., and Zviagina, B.B. (2004) The detailed structure and origin of clay minerals at the Cretaceous/Tertiary boundary, Stevns Klint (Denmark). *Clay Minerals*, **39**, 367–390.
Drits, V.A., Sakharov, B.A., Salyn, A.L., and Lindgreen, H. (2005) Determination of the content and distribution of fixed ammonium in illite-smectite using a modified X-ray diffraction technique: application to oil source rocks of western Greenland. *American Mineralogist*, **90**, 71–84.
Dudek, T. and Środoń, J. (1996) Identification of illite/smectite by X-ray powder diffraction taking into account the lognormal distribution of crystal thickness. *Geologica Carpathica-Series Clays*, **5**, 21–32.
Dyal, R.S. and Hendricks, S.B. (1950) Total surface of clays in polar liquids as a characteristic index. *Soil Science*, **69**, 421–432.
Guggenheim, S., Adams, J.M., Bain, D.C., Bergaya, F., Brigatti, M.F., Drits, V.A., Formoso, M.L.L., Galán, E., Kogure, T., and Stanjek, H. (2006) Summary of recommendations of nomenclature committees relevant to clay mineralogy: report of the Association Internationale pour l'Etude des Argiles (AIPEA) Nomenclature Committee for 2006. *Clay Minerals*, **41**, 863–877.
Hower, J. and Mowatt, T. C. (1966) The mineralogy of illites and mixed-layer illite/montmorillonites. *American Mineralogist*, **51**, 825–854.
Inoue, A., Meunier, A., and Beaufort, D. (2004) Illite-smectite mixed-layer minerals in felsic volcaniclastic rocks from drill cores, Kakkonda, Japan. *Clays and Clay Minerals*, **52**, 66–84.
Inoue, A., Lanson, B., Marques-Fernandes, M., Sakharov, B.A., Murakami, T., Meunier, A., and Beaufort, D. (2005) Illite-smectite mixed-layer minerals in the hydrothermal alteration of volcanic rocks: 1. One-dimensional XRD structure analysis and characterization of component layers. *Clays and Clay Minerals*, **53**, 423–439.
Jackson, M.L. (1975) *Soil Chemical Analysis – Advanced Course.* Published by the author, Madison, Wisconsin, USA.
Laird, D.A., Barak, P., Nater, E.A., and Dowdy, R.H. (1991) Chemistry of smectitic and illitic phases in interstratified soil smectite. *Soil Science Society of America Journal*, **55**, 1499–1504.
Lindgreen, H., Drits, V.A., Sakharov, B.A., Salyn, A.L., Wrang, P., and Dainyak, L.G. (2000) Illite-smectite structural changes during metamorphism in black Cambrian Alum shales from the Baltic area. *American Mineralogist*, **85**, 1223–1238.
Loucks, R.R. (1991) The bound interlayer H_2O content of potassic white micas: Muscovite-hydromuscovite-hydropyrophyllite solutions. *American Mineralogist*, **76**, 1563–1579.
McCarty, D.K., Sakharov, B.A., and Drits, V.A. (2008) Early clay diagenesis in Gulf Coast sediments: new insights from XRD profile modeling. *Clays and Clay Minerals*, **56**, 359–379.
Mehra, O.P. and Jackson, M.L. (1959) Constancy of the sum of mica unit cell potassium surface and interlayer sorption surface in vermiculite-illite clays. *Soil Science Society of America Proceedings*, **23**, 101–105.
Meunier, A. and Velde, B. (1989) Solid solutions in I/S mixed-layer minerals and illite. *American Mineralogist*, **74**, 1106–1112.
Meunier, A., Lanson, B., and Beaufort, D. (2000) Vermiculitization of smectite interfaces and illite layer growth as a possible dual model for illite-smectite illitization in diagenetic environments: a synthesis. *Clay Minerals*, **35**, 573–586.
Moore, D.M. and Reynolds, R.C. (1997) *X-ray Diffraction and the Identification and Analysis of Clay Minerals.* Oxford University Press, Oxford-New York, 378 pp.
Nadeau, P.H. and Bain, D.C. (1986) Composition of some smectites and diagenetic illitic clays and implications for their origin. *Clays and Clay Minerals*, **34**, 455–464.
Nadeau, P.H., Wilson, M.J., McHardy, W.J., and Tait, J. (1984) Interstratified clays as fundamental particles. *Science*, **225**, 923–925.
Newman, A.C.D. (1983) The specific surface of soils determined by water sorption. *Journal of Soil Science*, **34**, 23–32.
Orsini, L. and Remy, J.-C. (1976) Utilisation du chlorure de cobaltihexammine pour la determination simultanee de la capacite d'echange et des bases echangeables des sols. *Science du Sol*, **4**, 269–275.
Reynolds, R.C. (1985) *NEWMOD: A computer program for the calculation of one-dimensional patterns of mixed-layer clays*. R.C. Reynolds, Hanover, NH 03755, USA.
Sakharov, B.A., Lindgreen, H., Salyn, A.L., and Drits, V.A. (1999) Determination of illite-smectite structures using multispecimen X-ray diffraction profile fitting. *Clays and Clay Minerals*, **47**, 555–566.
Sato, T., Murakami, T., and Watanabe, T. (1996) Change in layer charge of smectites and smectite layers in illite/smectite during diagenetic alteration. *Clays and Clay Minerals*, **44**, 460–469.
Slonimskaya, M.V., Drits, V.A., Finko, V.I., and Salyn, A.L. (1978) The nature of interlayer water in fine-dispersed muscovites. *Izvestiya Akademii Nauk SSSR, seriya geologicheskaya*, **10**, 95–104 (in Russian).
Środoń, J. (1980) Precise identification of illite/smectite interstratifications by X-ray powder diffraction. *Clays and*

Clay Minerals, **28**, 401–411.
Środoń, J. (1984) X-ray powder diffraction identification of illitic materials. *Clays and Clay Minerals*, **32**, 337–349.
Środoń, J. (1999) Nature of mixed-layer clays and mechanisms of their formation and alteration. *Annual Reviews in Earth and Planetary Science*, **27**, 19–53.
Środoń, J. and McCarty, D.K. (2008) Surface area and layer charge of smectite from CEC and EGME/H_2O retention measurements. *Clays and Clay Minerals*, **56**, 155–174.
Środoń, J., Morgan, D.J., Eslinger, E.V., Eberl, D.D., and Karlinger, M.R. (1986) Chemistry of illite/smectite and end-member illite. *Clays and Clay Minerals*, **34**, 368–378.
Środoń, J., Andreoli, C., Elsass, F., and Robert, M. (1990) Direct HRTEM measurement of expandability of mixed-layer illite/smectite in bentonite rock. *Clays and Clay Minerals*, **38**, 373–379.
Środoń, J., Elsass, F., McHardy, W.J., and Morgan, D.J. (1992) Chemistry of illite-smectite inferred from TEM measurements of fundamental particles. *Clay Minerals*, **27**, 137–158.
Środoń, J., Eberl, D.D., and Drits, V.A. (2000) Evolution of fundamental particle-size during illitization of smectite and implications for reaction mechanism. *Clays and Clay Minerals*, **48**, 446–458.
Środoń, J., Kotarba, M., Biroň, A., Such, P., Clauer, N., and Wójtowicz, A. (2006a) Diagenetic history of the Podhale-Orava basin and the underlying Tatra sedimentary structural units (Western Carpathians): evidence from XRD and K-Ar of illite-smectite. *Clay Minerals*, **41**, 747–770.
Środoń, J., Clauer, N., Bana, M., and Wójtowicz, A. (2006b) K-Ar evidence for a Mesozoic thermal event superimposed on burial diagenesis of the Upper Silesia Coal Basin. *Clay Minerals*, **41**, 671–692.
Tiller, K.G. and Smith, L.H. (1990) Limitations of EGME retention to estimate the surface area of soils. *Australian Journal of Soil Research*, **28**, 1–26.
Velde, B. and Brusewitz, A.M. (1986) Compositional variation in component layers in natural illite/smectite. *Clays and Clay Minerals*, **34**, 651–657.
Viczián, I. (1997) Hungarian investigations on the 'Zempleni' illite. *Clays and Clay Minerals*, **45**, 114–115.
Weaver, C.E. (1965) Potassium content of illite. *Science*, **147**, 603–605.
Ylagan, R.F., Altaner, S.P., and Pozzuoli, A. (2000) Reaction mechanisms of smectite illitization associated with hydrothermal alteration from Ponza island, Italy. *Clays and Clay Minerals*, **48**, 610–631.

(*Received 3 November 2008; revised 1 May 2009; Ms. 0213; A.E. W.D. Huff*)